Abstract

A giant carbonate vein (≥50 m thick; fissure ridge travertines) and nearby travertine plateaus in the Semproniano area (Mt. Amiata geothermal field, southern Tuscany, Italy) are investigated through a multidisciplinary approach, including field and laboratory geochemical analyses (U/Th geochronology, C, Nd, O and Sr isotope systematics, REE abundances, and fluid inclusion microthermometry). The main aim of this work is to understand: (1) modes and rates for the growth of the giant vein and nearby travertine deposits within a Quaternary volcano-tectonic domain; (2) implications in terms of the CO_2 release; and (3) possible relationships with Quaternary paleoclimate and hydrological oscillations. Results show that the giant vein was the inner portion of a large fissure ridge travertine and grew asymmetrically and ataxially through repeated shallow fluid injections between >650 and 85 ka, with growth rates in the order of 10^{-2} and 10^{-3} mm/a. The giant vein developed mainly during warm humid (interglacial) periods, partially overlapping with the growth of nearby travertine plateaus. Estimated values of CO_2 leakage connected with the vein precipitation are between about $5x10^6$ and $3x10^7$ mol a^{-1} km^{-2}, approximately representing one millionth of the present global CO_2 leakage from volcanic areas. Temperatures estimates as obtained from O-isotopes and fluid inclusion microthermometry indicate epithermal conditions (90-50 °C) for the circulating fluid during the giant vein growth, with only slight evidence of cooling with time. Geochemical and isotope data document that the travertine deposits have developed mainly during Pleistocene warm humid periods, within a tectonically-controlled convective fluid circuit fed by meteoric infiltration and maintained by the regional geothermal anomaly hosted by the carbonate reservoir of the Mt. Amiata field.

Keywords: travertine, vein, CO_2 leakage, hydrothermalism, REE, C- O- Sr- Nd- isotopes, Quaternary climate, Tuscany.

Highlights

- Modes and rates for the growth of giant vein in fissure ridge travertines
- Geochemistry and geochronology of CaCO3 mineralizations.
- CO_2 leakage in hydrothermal areas.
- Feedbacks between neotectonics, hydrothermalism and paleoclimate oscillations

Growth of a Pleistocene giant carbonate vein and nearby thermogene travertine deposits at Semproniano, southern Tuscany, Italy

Gabriele BERARDI[1,*], Gianluca VIGNAROLI[2], Andrea BILLI[2], Federico ROSSETTI[1], Michele SOLIGO[1], Sándor KELE[3], Mehmet Oruç BAYKARA[4,7], Stefano M. BERNASCONI[5], Francesca CASTORINA[2,6], and Francesca TECCE[2], Chuan-Chou SHEN[4]

1 Dipartimento di Scienze, Sezione di Geologia, Università degli Studi di Roma Tre, Rome (Italy)
2 Istituto di Geologia Ambientale e Geoingegneria, C.N.R., Rome (Italy)
3 Institute for Geological and Geochemical Research, Research Centre for Astronomy and Earth Sciences, Hungarian Academy of Sciences, Budapest (Hungary)
4 High-Precision Mass Spectrometry and Environment Change Laboratory (HISPEC), Department of Geosciences, National Taiwan University, Taipei (Taiwan ROC)
5 ETH Zürich, Geological institute, Zürich, (Switzerland)
6 Dipartimento di Scienze della Terra, Sapienza Università di Roma, Rome (Italy)
7 Department of Geological Engineering, Pamukkale University, Denizli (Turkey)

* Corresponding author:
G. Berardi
Dipartimento di Scienze – Sezione di Geologia
Università degli Studi "Roma Tre"
L.go S.L. Murialdo, 1 – 00146 Rome (Italy)
Tel: +39 0657338082
gabriele.berardi@uniroma3.it

Abstract

A giant carbonate vein (≥50 m thick; fissure ridge travertines) and nearby travertine plateaus in the Semproniano area (Mt. Amiata geothermal field, southern Tuscany, Italy) are investigated through a multidisciplinary approach, including field and laboratory geochemical analyses (U/Th geochronology, C, Nd, O and Sr isotope systematics, REE abundances, and fluid inclusion microthermometry). The main aim of this work is to understand: (1) modes and rates for the growth of the giant vein and nearby travertine deposits within a Quaternary volcano-tectonic domain; (2) implications in terms of the CO_2 release; and (3) possible relationships with Quaternary paleoclimate and hydrological oscillations. Results show that the giant vein was the inner portion of a large fissure ridge travertine and grew asymmetrically and ataxially through repeated shallow fluid injections between >650 and 85 ka, with growth rates in the order of 10^{-2} and 10^{-3} mm/a. The giant vein developed mainly during warm humid (interglacial) periods, partially overlapping with the growth of nearby travertine plateaus. Estimated values of CO_2 leakage connected with the vein precipitation are between about $5x10^6$ and $3x10^7$ mol a^{-1} km^{-2}, approximately representing one millionth of the present global CO_2 leakage from volcanic areas. Temperatures estimates as obtained from O-isotopes and fluid inclusion microthermometry indicate epithermal conditions (90-50 °C) for the circulating fluid during the giant vein growth, with only slight evidence of cooling with time. Geochemical and isotope data document that the travertine deposits have developed mainly during Pleistocene warm humid periods, within a tectonically-controlled convective fluid circuit fed by meteoric infiltration and maintained by the regional geothermal anomaly hosted by the carbonate reservoir of the Mt. Amiata field.

Keywords: travertine, vein, CO_2 leakage, hydrothermalism, REE, C- O- Sr- Nd- isotopes, Quaternary climate, Tuscany.

1. Introduction

Thermogene travertines form through precipitation of $CaCO_3$ from supersaturated fluids usually generated and discharged in volcano-tectonic settings, often deposited in proximity of active geothermal springs or along open fissures (Pentecost, 1995; Ford and Pedley, 1996; Pentecost, 2005; Crossey et al., 2006). In addition to being important decorative and construction stones since at least the Roman time (Calvo and Regueiro, 2010), a renewed world-wide interest for thermogene travertine deposits resides in their importance to be potential analogs of long-term outflow from artificial CO_2 storages (Shipton et al., 2004; Bickle and Kampman, 2013; Burnside et al., 2013; Frery et al., 2015). Moreover, recent discoveries of large hydrocarbon reserves in subsalt porous microbial and travertine-like rocks along the Brazilian and Angolan margins of the Atlantic Ocean place thermogene travertines among the best exposed analogs of these hydrocarbon-reservoir rocks, which are hitherto known only from seismic data and well cores (e.g., Beasley et al., 2010; Rezende and Pope, 2015; Ronchi and Cruciani, 2015; Soete et al., 2015).

Travertines can show various deposit morphologies such as cascades, terrace mounds, fissure ridges, plateaus, and towers (Chafetz and Folk, 1984; Altunel and Hancock, 1993a, b; Pentecost, 1995; Pentecost, 2005). These morphologies are only partially dependent on the topography over which the travertines precipitate. Other factors such as (neo)tectonics (Altunel and Hancock, 1996; Hancock et al., 1999; Brogi, 2004a; Brogi and Capezzuoli, 2009; Brogi et al., 2010, 2012; De Filippis et al., 2013a; Ricketts et al., 2014; Maggi et al., 2015), climate oscillations (Sturchio et al., 1994, Rihs et al., 2000; Faccenna et al., 2008, De Filippis et al., 2012), earthquakes (Uysal et al., 2007, 2009; Brogi et al., 2014; Gradziński et al., 2014), and hydrological regimes (Priewisch et al., 2014; Crossey et al., 2015) have been proposed to influence travertine growth and morphology; however, the way how these and other factors control the travertine development and shape is still uncertain. It is, in particular, unclear what are the factors controlling travertine deposits, that are completely different in morphology and volume such as travertine fissure ridges and plateaus,

100 which can, nonetheless, form in close proximity during the same time span (e.g., De Filippis et al.,
101 2013b).

102 In this paper, we address the growth of travertine fissure ridges and plateaus. Fissure ridges are
103 deposits of travertines with an elongate mound shape characterized by a length between a few
104 meters and over 2000 m, and a main crestal fissure from which the travertine-feeding fluids gush
105 out (Chafetz and Folk 1984; Altunel and Hancock, 1993a,b, 1996; Çakır, 1999; Hancock et al.,
106 1999; Uysal et al., 2007, 2009; De Filippis et al., 2012, 2013a). Fissure ridges are usually formed by
107 two main travertine types: (1) the bedded travertine, which consists of a porous and stratified
108 deposit constituting the flanks (often clinostratified) and the bulk of the fissure ridge and (2) the
109 banded travertine, which consists of subvertical bands of sparry nonporous carbonate (usually
110 calcite, aragonite, or both) filling large veins that intrude the axial region of the fissure ridge. In
111 places, these veins can also develop as sill-like structures along the beds of the bedded travertine or
112 host rocks (Uysal et al., 2007; Gratier et al., 2012). Travertine plateaus, in contrast, are
113 characterized by massive and large deposits consisting of sub-horizontal to gently-clinostratified
114 travertine beds usually filling a tectonic or morphological depression and producing no prominent
115 topography (Faccenna et al., 2008; De Filippis et al., 2013a).

116 Tuscany (Fig. 1), central Italy, is a region characterized by Neogene-Quaternary formation of
117 extensional basins, widespread magmatism, associated contact metamorphism, hydrothermalism
118 and ore mineralization, and also numerous thermogene travertine deposits (Marinelli et al., 1993;
119 Serri et al., 1993; Barberi et al., 1994; Carmignani et al., 1994; Dini et al., 2005; Gandin and
120 Capezzuoli, 2008; Brogi and Capezzuoli, 2009; Rossetti et al., 2008, 2011). Travertine deposition in
121 Tuscany has occurred near highly-productive geothermal areas (Larderello-Travale and Mt. Amiata;
122 Batini et al., 2003), where endogenous fluids permeate Meso-Cenozoic carbonate reservoirs and
123 mix before feeding thermal springs and CO_2 emission centers (e.g., Minissale, 2004). Both
124 travertine fissure ridges and plateaus are documented in Tuscany. In particular, studied fissure
125 ridges are exposed in the Rapolano Terme (e.g., Brogi and Capezzuoli, 2009; Guo and Riding,

126 1999) and Castelnuovo dell'Abate (Rimondi et al., 2015) localities (Fig. 1b), where banded
127 travertine forms centimeters-to-meters thick veins within meters-sized elongate mounds accreted
128 over a restricted time interval between Pleistocene and Holocene times.

129 We focus our study on travertines exposed in the village of Semproniano (northern Albegna
130 basin), which is built on top of a hill at an altitude of 620 m. Semproniano is located only about 15
131 km southward of the Mt Amiata Pleistocene volcanic district and 9 km from the Saturnia thermal
132 spring (Figs. 1 and 2), where active travertine deposition still occurs. The Semproniano village lies
133 on a travertine fissure ridge, a composite carbonate vein (≥50-m-thick) consisting of subvertical
134 banded travertine (Capezzuoli et al., 2013), which crops up from the surrounding host carbonate
135 rocks (Paleogene). Other travertine deposits or carbonate mineralizations, including travertine
136 plateaus, small veins, and bedded travertines, are exposed within a few kilometers from the
137 Semproniano village (Fig. 3a). The origin and growth modes of these deposits and mineralizations
138 in the Semproniano area are unknown and the main driving factors (e.g., tectonics, paleohydrology,
139 paleoclimate, etc.) as well. Moreover, absolute dating of these travertines is missing, thus making
140 very difficult the regional correlation among these deposits as well as between the deposits
141 themselves and the dated tectonic, volcanic, and paleoclimate events in the region.

142 The coexistence of different nearby $CaCO_3$-mineralizations and travertine deposits in a region
143 of recent tectonic and volcanic activity makes the Semproniano area an excellent case study to
144 understand the nature of those carbonates deposits. Using a multidisciplinary approach consisting of
145 geological, structural, geomorphologic, and geochemical methods (including fieldwork, remote
146 observations, U/Th dating, C- Nd- O- and Sr-isotope systematics, rare Earth element (REE)
147 abundances, and fluid inclusion microthermometry), this study is aimed at understanding the
148 development of the different travertine bodies (vein and plateau type), their mutual relationships,
149 and the feedback relationships between travertine deposition and driving factors such as tectonics,
150 volcanisms, and paleoclimate. The main novelty of this work concerns growth modes and rates of
151 the Semproniano fissure ridge and implications for the associated CO_2 leakage. In addition, our

results provide insights at regional scale concerning the late Quaternary hydrothermal and tectonic activity of southern Tuscany.

2. Geological setting

Southern Tuscany is located in the inner sector (western) side of the northern Apennine chain (Fig. 1), which is a Cenozoic NW-SE-trending orogenic belt developed through a general eastward migration of thrust sheets in a classical piggy back sequence toward the Adriatic foreland (e.g., Patacca et al., 1990; Cipollari and Cosentino, 1995; Massoli et al., 2006). In Tuscany, post-orogenic extension and collapse of the previously formed orogenic belt started in late Miocene time, while, toward the east, the belt was still under a compressional regime (e.g., Malinverno & Ryan, 1986; Dewey 1988; Jolivet et al., 1998; Cavinato and De Celles, 1999; Pauselli et al., 2006). The extensional process generated normal faults that dismantled the previously-formed fold-thrust belt (e.g. Carmignani et al., 1994; Keller et al., 1994; Barchi et al., 1998; Jolivet et al., 1998; Collettini et al., 2006) and produced significant crustal thinning (present-day crust thickness is about 22-24 km; Locardi and Nicolich, 1988; Billi et al., 2006) as well as the development of sedimentary basins, magmatic provinces, and diffuse volcanism (Serri et al., 1993; Serri, 1997; Peccerillo, 2003). Fossil and active, structurally-controlled hydrothermal mineralizations are widespread evidence of the interaction between hydrothermal systems and extensional faults (e.g., Barberi et al., 1994; Buonasorte et al., 1988; Chiarabba et al., 1995; Gianelli et al., 1997; Batini et al., 2003; Bellani et al., 2004; Annunziatellis et al., 2008; Brogi, 2008; Liotta et al., 2010; Rossetti et al., 2011; Vignaroli et al., 2014).

Southern Tuscany (Fig. 1) is characterized by main NW-SE-trending and minor NE-SW-trending Miocene-to-Quaternary sedimentary basins formed during post-orogenic extensional processes and bounded by extensional-to-transtensional structures (Martini and Sagri, 1993; Liotta, 1994; Pascucci et al., 2006; Brogi and Liotta, 2008; Brogi, 2011; Brogi et al., 2013; 2014; 2015; Marroni et al., 2015). These structures include the Tevere-Paglia, Siena-Radicofani, and Albegna

178 basins. The Semproniano thick vein and surrounding travertine deposits are located in the Albegna
179 basin, which consists of a NE-SW-trending tectonic depression bounded to the north and southeast
180 by the volcanic districts of the Mt Amiata and Vulsini Mts, respectively (Fig. 1). The magmatic
181 activity (or part of it) of the Mt Amiata district is dated to 300-190 ka according to Cadoux and
182 Pinti (2009) and to 300-225 ka according to Laurenzi et al. (2015), whereas the activity (or part of
183 it) of the Vulsini Mts district is dated to 590-127 ka according to Nappi et al. (1995).

184 The geological setting of the Albegna basin is characterized by the presence of metamorphic
185 and non-metamorphic tectonic units stacked during the formation of the Apennines fold-thrust belt.
186 From bottom to top, these units are as follows (e.g., Carmignani et al., 2013): (1) low-grade
187 metamorphic rocks of the Tuscan Metamorphic Complex; (2) Upper Triassic to Oligocene
188 kilometers-thick sedimentary succession composed by basal evaporites followed by shelf
189 carbonates and marls (Tuscan Nappe); (3) Jurassic to Eocene ophiolite-derived clays and marls
190 succession (Ligurian Domain); and (4) Upper Miocene to Pleistocene terrigenous post-orogenic
191 deposits. The latter consist of fluvio-lacustrine deposits and marine clays that deposited in subsiding
192 areas concomitantly with the regional tectonic extension (Zanchi and Tozzi, 1987; Bonazzi et al.,
193 1992; Bossio et al., 2004).

194 In the Albegna basin, travertine deposits unconformably lie on top of the Neogene-Pleistocene
195 deposits (Zanchi and Tozzi, 1987; Martelli et al., 1989; Bosi et al., 1996). The travertine deposition
196 occurred in distinct phases and over a long time interval (Bosi et al., 1996). In particular, based on
197 the travertine morphological and stratigraphic characters, Bosi et al. (1996) proposed a travertine
198 deposition spanning from Messinian to Holocene times. In particular, Bosi et al. (1996) suggested
199 that the travertines of the Semproniano area deposited during Pliocene time, whereas other authors
200 considered them as early Pleistocene in age (Zanchi and Tozzi, 1987). The lack of absolute
201 radiometric ages restricts the full understanding of these travertine deposits and their relationships
202 with the hydrothermal and tectonic activity in the Albegna basin.
203

3. Methods and Results

3.1. Geology and geomorphology

We performed a field-based study on the geology, geomorphology, and structural setting of the travertine deposits located in the Semproniano area, namely: the (1) Semproniano ridge, (2) I Vignacci, (3) Poggio Semproniano, and (4) Poggio i Piani deposits (Figs. 2-5). We focused this study on the recognition of different travertine morphotypes (e.g., plateaus vs. fissure ridge travertines), on the relationships between travertine deposits and host rocks, and on the deformation features affecting the travertine deposits.

The study area is characterized by a set of post-orogenic Pliocene-Quaternary continental and marine sedimentary deposits (including the studied travertines) that unconformably rest on top of the Apennine stacked units (e.g., Bonciani et al., 2005; Brogi, 2008; Brogi and Fabbrini, 2009). The travertine plateaus (Poggio Semproniano and Poggio i Piani), in particular, unconfomably lie over Pliocene-Quaternary deposits and over the Scaglia Toscana Fmt. of the underlying Tuscan Nappe (Fig. 4a) which host the Semproniano fissure ridge (Fig. 2). The Poggio Semproniano deposit occupies the top portion of a triangular hill that is almost 700 m high (Fig. 3). The hill is tabular with a terrace-like top surface marked by a peripheral rim that runs all around the terraced deposit and delimits the terrace itself from the steep flanks of the hill. At the foot of these escarpments, the contact between the travertine deposit and the surrounding units is often covered by debris constituted by alluvial and eluvial deposits. The travertine body has dimensions of around 1300 m in the NW-SE direction and 700 m in the N-S direction, and has a maximum vertical thickness of about 200 m (Figs. 2 and 3). The travertine depositional fabric consists of piano-parallel centimeters-thick beds of whitish lime-mudstone with homogeneous porosity due to the presence of microbialites. Millimeter to centimeter-sized karst dissolution cavities are also present (Fig. 4c). On the eastern flank, the travertine beds of the Poggio Semproniano plateau and the underlying marly deposits of the Tuscan Nappe are pervaded by a set of cm-thick subvertical veins striking NW-SE, filled by white sparry carbonate.

The Poggio i Piani deposit is very similar to the one of Poggio Semproniano. Poggio i Piani is a terraced triangular hill with maximum elevation around 630 m. Also here, the travertine deposit is characterized by an outer sharp rim that runs all around the terraced deposit and delimits the terrace itself with the steep flanks of the hill. The deposit is tabular and sub-horizontal with sedimentary features similar to the ones described for Poggio Semproniano (Figs. 4c, d, e). The dimensions of the Poggio i Piani travertine plateau are about 500 m in the NW-SE direction and 450 m in the N-S direction with a maximum thickness of 35 m (Fig. 2). A narrow N10°-trending valley with a minimum elevation of about 500 m separates the Poggio Semproniano and Poggio i Piani hills (Fig. 3).

The Semproniano ridge is separated from the Poggio Semproniano and Poggio I Piani deposits by a narrow NW-SE-trending valley with a minimum elevation of about 500 m (Fig. 3). The Semproniano ridge crops out from the top of a NW-SE-elongate domed hill with maximum altitude around 620 m a.s.l. and about 1000 m long and 400 m wide. The central part of the Semproniano ridge, constituted by banded sparry travertine with a total thickness of more than 50 m, is characterized by complex geometries such as V-like-shaped (Fig. 5e) or crosscutting carbonate bands that are up to about 2 cm thick. The sparry subvertical bands of carbonate form a unique, composite and uninterrupted vein that we call the Semproniano giant vein for its large thickness of more than 50 m. The southwestern flank of the ridge is characterized by the presence of sub-horizontal bedded travertine leaning over the sub-vertical banded travertine (Fig. 5f). The bedded travertine is characterized by sub-horizontal brownish centimeters-thick beds (Fig. 5g), shrubs, and laminations affected, in places, by millimeters-to-centimeters-sized cavities of depositional and post-depositional (karst) origin. In some cases, the porous bedded travertine appears to be pervaded by bed-parallel veins (Fig. 5h and 5i). In the external part of the southwestern flank of the giant vein, at an altitude of about 580 m a.s.l, a set of sub-vertical centimeters-thick carbonate veins cut through the marly carbonates of the Scaglia Toscana Fmt. (Fig. 5j, k), which is the host rock of the giant vein travertine (Fig. 2).

256 The I Vignacci deposit crops out about 800 m to the northwest of the Semproniano ridge,
257 exactly along the NW-SE prolongation of the Semproniano hill and ridge (Figs. 2 and 3). I Vignacci
258 travertine is located at an altitude of about 430 m a.s.l., the lowest reached of the studied travertines.
259 I Vignacci travertine deposit is small and it is characterized by banded travertine with subvertical
260 NW-SE-striking bands. These bands cut through the surrounding sub-horizontal beds of the Scaglia
261 Toscana Fmt. Geometrical attitude and location of I Vignacci outcrop suggest a structural and
262 geometric continuity with the Semproniano ridge (Figs. 2 and 3).
263 From a tectonic point of view, the travertine deposits are cross-cut by two main subvertical fault
264 systems, one striking ca. E-W and one striking N-S (Figs. 2 and 6). In particular, we recognized that
265 the E-W-striking fault system cuts through the northern portion of the Poggio Semproniano
266 travertine plateau (Fig. 6a). It consists of meter-thick damage zone defined by fault slip surfaces and
267 secondary, subparallel, fracture network (Fig. 6b). A pitch smaller than 15° or greater than 165°
268 have been measured for most slickenlines and abrasive striations occurring on fault planes (Fig. 6c).
269 The kinematic indicators observed on the fault surfaces are mainly represented by synthetic shear
270 fractures within the damage zone (Riedel shear planes) and they are consistent with right-lateral
271 strike-slip movements. The N-S-striking fault system passes along the valley that separates the
272 Poggio Semproniano and Poggio i Piani travertine deposits (Fig. 2). We identified this set of faults
273 as affecting the travertine deposits of the Semproniano ridge and cut through the banded travertine
274 of the Semproniano fissure ridge (Fig. 6a). Within the ridge, the fault system is characterized by a
275 0.5 m-thick damage zone and several speleothem-filled fracture networks cutting through the
276 banded travertine (Fig. 6d). When observed, abrasive striations on fault planes show a pitch of
277 about 60-70°. Geometrical relationships between faults and secondary fractures are consistent with
278 an extensional movement (associated to a left-lateral movement) lowering the Poggio Semproniano
279 travertine deposit.
280
281 ***3.2. U/Th geochronology***

We dated nineteen samples from the $CaCO_3$ mineralizations in the study area (Tables 1, 2, and S1), namely from Semproniano (thirteen samples from the giant banded vein, bedded travertines, and one subordinate vein), I Vignacci (one sample from the banded travertine), Poggio Semproniano (three samples from bedded travertines and veins), and Poggio I Piani (one sample from bedded travertines). The analytical methods (α spectrometry and mass spectrometry) are described in the Appendix.

Banded travertine samples from Semproniano Village (SP1) and I Vignacci (VI1) are characterized by a $^{230}Th/^{234}U$ activity ratio higher than 1 and, therefore, by ages higher than the limit of the U/Th method in α spectrometry (c. 350 ka). The bedded travertine exposed on the south-western flank of the Semproniano giant vein (SP11) is characterized by a moderate detrital contamination ($^{230}Th/^{232}Th$ activity ratio = 7.148 ± 0.251) and by a corrected $^{230}Th/^{234}U$ activity ratio of 0.878 ± 0.051, indicating an age of 214 +50/-37 ka. A subordinate carbonate vein (SP16) cutting through the Scaglia Toscana Fmt. (Tuscan Nappe) in the external south-western flank of the Semproniano giant vein is characterized by a $^{230}Th/^{232}Th$ activity ratio of 12.564 ± 1.987 and by a corrected $^{230}Th/^{234}U$ activity ratio of 0.641 ± 0.064. Calculated age for this sample is 104 ± 16 ka. A bedded travertine sample collected in the southern part of Poggio Semproniano plateau (PO2; Fig. 4b) is characterized by a $^{230}Th/^{234}U$ activity ratio of 0.818 ± 0.039. The resulting age is 171 ± 19 ka. Two samples of calcite-filled veins (SP3 and SP10) cutting through the bedded travertine of Poggio Semproniano and the underlying Scaglia Toscana Fmt. are characterized by a $^{230}Th/^{234}U$ activity ratio of 0.340 ± 0.052 and 0.299 ± 0.023, respectively. The related ages are 43 ± 8 ka and 39 ± 4 for the SP3 and SP10 samples, respectively. A sample of bedded travertine from Poggio I Piani plateau (PP1; Fig. 4e) is characterized by a $^{230}Th/^{234}U$ activity ratio of 0.857 ± 0.028 and a resulting age of 198 ± 18 ka.

To understand the spatio-temporal growth of the Semproniano giant banded vein, we dated eleven samples from this vein along a 5m transect across the vein (Fig. 6), and one sample (SP12) from the upper part of the transect (Figs. 5e and 7) by mass spectrometry (Fig. 7 and Tables 2 and

S1). We obtained, ages between 86 ka to 646 ka (Fig. 7), with only one sample being older than the resolution of the method (> c. 800 ka). Radiometric ages along the transect do not vary systematically. In other words, the oldest samples are not located within the inner or external portions of the vein to indicate its antitaxial or syntaxial growth. The three oldest samples (i.e., c. 646, 613, and >800 ka) occur in separate inner portions of the vein and are divided by younger carbonates. (Fig. 7). The oldest samples have lager errors caused by proximity to secular equilibrium, whereas the youngest ages are characterized by smaller errors (Table 2).

3.3. C- and O-isotopes and parental fluid thermometry from O-isotopes

We performed $\delta^{13}C$ and $\delta^{18}O$ analyses on fifty one samples (banded and bedded travertines, calcite veins) from the Semproniano area (Tables 1 and 3). Details on the analytical procedure are provided in the Appendix. Oxygen and carbon isotopes are reported with respect to V-PDB. All analyzed samples are characterized by positive values of $\delta^{13}C$ (between 3.2 and 10.5‰) and negative values of $\delta^{18}O$ (between -14.6 and -7.6‰) (Table 3). Results, in particular, are clustered around 8‰ for $\delta^{13}C$ and around -11‰ for $\delta^{18}O$ (Fig. 8b).

Semproniano Village. Samples of banded travertine from the Semproniano veins are characterized by $\delta^{13}C$ values between 3.2 and 10.5‰ (V-PDB) and by $\delta^{18}O$ values between -14.6 and -7.6‰ (V-PDB). Samples from the associated bedded travertine are characterized by $\delta^{13}C$ values between 5.3 and 9.9‰ (V-PDB) and by $\delta^{18}O$ values between -9.8 and -8.2‰ (V-PDB).

I Vignacci. The sample from the banded travertine of I Vignacci (sample VI1) is characterized by a $\delta^{13}C$ of 3.7‰ (V-PDB) and a $\delta^{18}O$ of -9.6‰ (V-PDB).

Poggio Semproniano. Samples of bedded travertine from Poggio Semproniano are characterized by values of $\delta^{13}C$ between 5.7 and 7.1‰ (V-PDB) and values of $\delta^{18}O$ between -11.4 and -8.1‰ (V-PDB). Calcite-filled veins pervading the bedded travertine and the underlying underlying Scaglia Toscana Fmt. (Samples SP3, SP10) at the bottom of the Poggio Semproniano travertine plateau are

characterized by $\delta^{13}C$ values between 7.1 and 8.4‰ (V-PDB) and $\delta^{18}O$ values between -11.5 and -10.7‰ (V-PDB).

Poggio i Piani. One sample from the bedded travertine (sample PP1) of Poggio i Piani is characterized by a $\delta^{13}C$ of 6.5‰ (V-PDB) and a $\delta^{18}O$ of -11.6‰ (V-PDB).

We focused particular attention to the Semproniano giant vein by collecting two transects across it (samples SP14/03 to SP14/04 and SP14/08 to SP14/34) and three further samples in the adjacent bedded travertine (samples SP11, SP14/05, SP14/06) (Table 3). Banded travertines collected along the two transects show a wide variability. Samples from the first transect (samples SP14/03 to SP14/16), in particular, are characterized by $\delta^{13}C$ values comprised between 5.3 and 9.7‰ (and $\delta^{18}O$ values comprised between -12.8 and -9.0‰. Samples from the second transect (samples SP14/17 to SP14/34) are characterized by $\delta^{13}C$ values comprised between 3.2 and 10.2‰ and $\delta^{18}O$ values comprised between -12.6 and -7.6‰. Samples from the bedded travertine located along the flanks of the Semproniano giant vein are characterized by $\delta^{13}C$ values comprised between 5.3 and 9.9‰ and $\delta^{18}O$ values comprised between -9.8 and -8.2 ‰. Samples from the two transects don't show any pattern in O and C isotopic values along the Semproniano giant vein.

We calculated the paleo-temperature of the mineralizing parental fluids applying the equation of Kele et al. (2015) to the entire $\delta^{18}O$ dataset (Table 3 and Fig. 8c) and using the present $\delta^{18}O$ of the the Saturnia spring hydrothermal waters (-6.4‰ V-SMOW), whose active source is located 9 km to the south of the Semproniano giant vein. We assume that the oxygen isotope composition of the palaeosprings was similar to those of the current Saturnia spring. The banded travertines of the Semproniano giant vein yield temperatures between 34 ± 2 and 71 ± 7 °C, with the majority in the range comprised between 45 and 60 °C. The bedded travertines associated with the giant vein give temperatures between 35 ± 2 and 43 ± 3 °C, whereas the banded travertine sample from I Vignacci sample yields a temperature of 42 ± 3°C. The Poggio Semproniano plateau samples yield temperatures of 36 ± 2 and 53 ± 5 °C, for the bedded travertine, and 49 ± 4 and 53 ± 5 °C, for the

358 calcite veins. The bedded travertine from Poggio I Piani a temperature of 53 ± 5 °C. There is no
359 correlation scheme between ages and temperature of precipitation (Fig. 8d). In particular, there is no
360 systematic trend of decreasing temperature with younger ages of deposition.
361
362 ***3.4. Sr- and Nd-Isotopes and rare Earth elements***
363 We performed Strontium, REE, and Yttrium (Y; REE + Yttrium = REY) concentration analysis,
364 and Strontium and Neodymium isotope measurements to understand the subsurface circuit of
365 hydrothermal fluids (e.g., Ederfield and Greaves, 1982; McLennan, 1989; Webb et al., 2000; Uysal
366 et al., 2007; 2009). The analytical procedures and protocols are detailed in the Appendix; results are
367 reported in Tables 4 and S2 and Fig. 9.
368 We observed a variable Sr concentration, comprised between 105.3 to 4956.3 mg/kg. The mean
369 value (3200 mg/kg) is in the range of Sr contents of most travertines in central Italy (Minissale,
370 2004). Sr-isotope ratios range from 0.708277 to 0.708527. The banded travertine from the
371 Semproniano giant vein (SP12, SP14/18 and SP14/28), the banded travertine from I Vignacci (VI1),
372 and the calcite vein from Poggio Semproniano (SP3 and SP10) are characterized by the highest Sr
373 concentrations, between 1125.9 and 4956.3 mg/kg. On the contrary, the bedded travertine from the
374 flanks of the Semproniano giant vein (SP11, SP14/06, SP17) and the bedded travertines from
375 Poggio Semproniano (SP9, PO1, PO2) are have the lowest Sr concentrations, between 105.3 and
376 787.3 mg/kg.
377 The Nd-isotope composition of one bedded travertine from the flanks of the Semproniano giant
378 vein (SP14/06), one banded travertine from I Vignacci (VI1), and one calcite vein from Poggio
379 Semproniano (SP3) show values comprised in a narrow range between 0.512253 and 0.512330
380 (Table 4).
381 We determined REY concentrations of the banded travertine from the Semproniano giant vein
382 (SP14/18), of the bedded travertine sample from the flanks of the Semproniano giant vein
383 (SP14/06),of the banded travertine sample from I Vignacci (VI1) of the bedded travertine sample

(PO1) and of calcite vein (SP3) from Poggio Semproniano. We normalized the REY concentrations against PAAS (Post-Archean Austrian Shale; McLennan, 1989; Fig. 9 and Table S2). The REY concentrations are highly variable (ΣREE = 0.08-18.6), resulting significantly lower than PAAS (Fig. 9). The main features of REY patterns are (Fig. 9): (i) relative depletion of the light rare Earth elements (LREE = 0.1-0.71, with the exclusion of sample VI1); (ii) variable enrichment of the heavy rare Earth elements (HREE as NdN/YbN = 1.9- 0.07, according to Webb and Kamber, 2000); (iii) strongly superchondritic Y/Ho ratio (38.3 -221.3) characterized by a huge positive Y spike in the pattern; (iv) positive Gd anomaly for sample SP14/06 and VI1; (v) consistent negative Ce anomaly (Ce/Ce* = 0.30-0.94; Table S2).

3.5. Fluid inclusion microthermometry

Fluid inclusion microthermometry is the best direct technique to understand and reconstruct the physical and chemical properties of the mineralizing fluids; however, fluid inclusion studies on travertines are rare (Słowakiewicz 2003; Gibert et al., 2009; El Desouky et al., 2015; Raimondi et al., 2015) due to some difficulties inherent to travertines such as: (1) scarce occurrence and small size of inclusions (Pentecost 2005); (2) inclusion metastability often causing failing in bubble nucleation upon cooling from the trapping conditions to room temperature (Diamond, 2003); and (3) inclusion anelastic stretching and decrepitation that can cause difficulties in performing microthermometric analyses; (4) double refraction of calcite (Bodnar, 2003).

Unfortunately only one sample contained fluid inclusions suited for microthermometry (Fig. 10a). It consists of elongate calcite crystals, containing numerous two-phase (Liquid+Vapor or L+V) liquid-rich fluid inclusions 5 to 50 μm long and a constant V/L ratio for all the analyzed structures (Figs. 10b-10d). Fluid inclusions occur both as primary isolated and as pseudosecondary in small planes that do not cross the crystal rims. The inclusion shape is variable. We recognized, in particular, two main types of inclusions: (1) flat irregular (Figs. 10c and 10d) and (2) polygonal (Fig. 10b).

As it is shown in Fig 10(f), Tm_{ice} values (i.e., the temperature of ice melting from which salinity is deduced) range between 0.0 and +4.8 °C, but are mostly concentrated around 0-1 °C. Being very small systems, fluid inclusions may exhibit metastable behaviour and metastable ice crystals can persist at temperatures as high as +6,5°C (Roedder, 1967) (Fig. 10f). From these data we can conclude that the fluid consists of pure water. Homogenization temperature (Th) values range between 57 and 105°C, with a maximum around 70-90 °C (Fig. 9g). No pressure correction is required for these homogenization temperature values as the analyzed sample precipitated in a very shallow environment represented by the giant vein. Our microthermometric results (Fig. 10e) are consistent with the ones obtained by Capezzuoli et al. (2013), who obtained temperatures between 65 and 95 °C and 0.2 wt% NaCl eq.

4. Discussion

4.1. A long-lived giant vein

The thick and continuous sequence of travertine sparry subvertical bands (the giant vein) in the Semproniano village accompanied by bedded travertine on its flanks and by veins in the Tuscan Nappe host rock suggest that the Semproniano giant vein represent the central portion of a fossil fissure ridge travertine larger than, but similar to those known in several other hydrothermal areas such as Turkey (e.g. Denizli Basin; Altunel and Hancock 1993a,1993b, 1996; Uysal et al., 2007,2009; De Filippis et al., 2012, 2013a), U.S.A. (e.g. Mammoth Hot Springs and Bridgeport; Hancock et al., 1999; De Filippis and Billi, 2012), Italy (e.g. Rapolano, Castelnuovo dell'Abate, and Tivoli; Guo and Riding, 1999; Brogi, 2004a; Brogi and Capezzuoli, 2009; De Filippis et al., 2013b; Rimondi et al., 2015), and elsewhere (De Filippis et al., 2012). Most fissure ridge travertines are volumetrically dominated by bedded travertines occurring mainly along the flanks and partially along the axial portion of the ridges, whereas the banded travertine is normally confined within a narrow band along the ridge axis. In the Semproniano case, although we have no record on the amount of eroded bedded travertine over time (since about 650 ka), the ridge seems to be

436 characterized by a predominance of banded travertine (i.e., the giant vein) with only small slabs (at
437 present) of bedded travertine on its flanks.

438 We consider the Semproniano vein as a giant structure characterized by a minimum thickness of
439 50 m larger than any one we found in the published literature. Thus the Semproniano giant vein is
440 probably the thickest continuous vein (i.e., no relics of host rock are interspersed across the
441 Semproniano giant vein) so far documented in the geological literature. Very thick veins (i.e.,
442 banded travertine) are common in many fissure ridge travertines (e.g. Uysal et al., 2007, 2009; De
443 Filippis et al., 2012), but their thickness (at least that of the continuous portion of banded travertine)
444 is normally at least one order of magnitude smaller than that of Semproniano. For instance, the
445 Akköy fissure ridge in the Denizli basin (Turkey) is known as one of the largest and thickest fissure
446 ridges on the Earth. This fossil structure is well visible in its inner portion thanks to the presence of
447 numerous quarries. In the quarries, the Akköy ridge is characterized by inner veins that are less than
448 10 m thick (i.e., considering only continuous veins; De Filippis et al., 2012).

449 Very thick veins pervading rocks are common in different settings (e.g., metamorphic rocks),
450 but all these occurrences are characterized by non-continuous veins, with relics of host rock
451 interspersed across the veins. Quartz veins of a thickness comparable to the one of Semproniano
452 were described by Bons (2001) and Yilmaz et al. (2014). In both instances, the veins have
453 thicknesses close to 50 m but, unlike the Semproniano structure, these quartz veins are
454 characterized by wall rock inclusions.

455 We interpret the giant thickness of the Semproniano vein as due to two main factors: (1) the
456 shallow emplacement of this vein and therefore the limited confining pressure, which would have
457 otherwise limited the lateral expansion of the vein in a deeper case. Although we do not know the
458 exact depth of formation, most veins along fissure ridge travertines are typically formed only at a
459 few meters depth at the most (De Filippis et al., 2012, 2013a); (2) the second factor is the unique
460 longevity of the hydrothermal activity, which lasted at least 600 ka. This is much longer than what

461 is reported by other studies of fissure ridge travertines which are typically around 10^4 a (e.g.,
462 Altunel and Karabacak, 2005; Uysal et al., 2007, 2009).
463
464 ***4.2. Rate and mode of vein growth***
465 The Semproniano giant vein grew between about >650 and 85 ka. Considering 50 m as the vein
466 total thickness, the average growth rate around can be estimated to be 8 x 10^{-2} mm/a. The three
467 inner sectors of the giant vein can also be considered separately according to age groups: sector A,
468 between samples SP14/25 and SP14/23; sector B, between samples SP14/23 and SP14/20; and
469 sector C, between samples SP14/20 and SP14/18 (Fig. 7b). With distance between the dated
470 samples in each sector and the age difference, we obtain average growth (i.e., thickening) rates of
471 about 7 x 10^{-3}, 2 x 10^{-2}, and 6 x 10^{-3} mm/a for sectors A, B, and C, respectively. We therefore
472 assume that the Semproniano giant vein grew with average rates ranging between ca. 10^{-2} and 10^{-3}
473 mm/a. These rates are consistent with previously-estimated rates for banded travertines within
474 fissure ridges located elsewhere (about 10^{-2} mm/a; Uysal et al., 2007; Mesci et al., 2008; Gratier et
475 al., 2012; De Filippis e al., 2013a; Frery et a., 2015). This result confirm that the giant thickness of
476 the Semproniano vein is not related to a fast growth rate but rather to the duration of hydrothermal
477 activity, which is significantly larger than veins in other fissure ridges (e.g., Altunel and Karabacak,
478 2005; Uysal et al., 2007, 2009).
479 The age distribution along the transect shows that the oldest samples are located neither at the
480 lateral ends of the giant vein nor at its central part indicating that the vein did not grow in a
481 syntaxial or antitaxial fashion (Bons et al., 2012). The three oldest samples (i.e., c. 646, 613, and
482 >800 ka; Fig. 7b) occur in separate inner portions of the vein showing that it grew asymmetrically
483 and ataxially (Passchier and Trouw, 1996; Bons et al., 2012) with no systematic growth direction
484 and no systematic age sequence. Based on our data, we hypothesize an accordion-like mode of
485 growth through multiple events of crack-and-seals pulses, which is well supported by the U/Th ages.
486 This growth mode for the Semproniano giant vein is somewhat different from models proposed for

fissure ridge structures (e.g., Hancock et al., 1999; Brogi and Capezzuoli, 2009) characterized by banded travertine forming injection veins and sill-like structures filling diffused fractures within the bedded travertine. The Semproniano giant vein, in fact, defines a singular structure that grew within the same horst rock over a long time, maintaining the same orientation.

4.3. Hydrothermal parental fluids

C- and O-isotope data show that the Semproniano giant vein is of thermogene origin (Pentecost, 2005). All analyzed samples are characterized by positive $\delta^{13}C$ and negative $\delta^{18}O$ values (Table 3, Fig. 7b), indicating mixing between hydrothermal parental fluids and meteoric waters and with a significant contribution of CO_2 originating from limestone decarbonation (Gonfiantini et al., 1968; Guo et al., 1996: Billi et al., 2007). Our stable isotope data are in the range typical of thermogene travertines deposited by present-day thermal springs of central Italy (Minissale, 2004; Gandin and Capezzuoli, 2008).

$\delta^{13}C$ values of travertines have been used to determinate the original signal of $\delta^{13}C_{CO2}$ applying the empirical equation of Panichi and Tongiorgi (1976) and the theoretical equation of Bottinga (1968) (Table 3). According to the equation of Panichi and Tongiorgi (1976), the $\delta^{13}C_{CO2}$ values are comprised between -6.7 and 2.1 ‰ (V-PDB), while according to the equation of Bottinga (1968), the $\delta^{13}C_{CO2}$ values are comprised between -5.4 and 3.5 ‰ (V-PDB). Those results confirm a mixing between CO_2 originated from limestone decarbonation with CO_2 of igneous origin (e.g. Turi, 1986; Minissale, 2004; Kele et al., 2011).

The O-isotope composition allowed us to estimate the parental fluid temperatures using the water oxygen isotopic composition of modern springs. In the case of the Semproniano giant vein, calculated temperatures span between about 34 ± 2 and 71 ± 7°C, with the majority of data comprised between 46 and 60 °C (Table 3, Fig. 8c). The validity of these temperature estimates are confirmed by the fluid inclusion microthermometric data on sample SP12 yielding temperatures between 70 and 90 °C (Fig. 10). This supports the assumption that the oxygen isotope composition

513 of the hydrothermal fluid did not change substantially through time. Fluid inclusion data also show
514 that the giant vein parental fluid was constituted by almost pure water.

515 The lack of correlation between ages and precipitation temperatures in the giant vein (Fig. 8d),
516 indicate no systematic and linear cooling of hydrothermal parental fluids with time. This differ from
517 the study of Rimondi et al. (2015), on the Pleistocene Castelnuovo dell'Abate travertines on the
518 northern flank of the Mt. Amiata volcano which showed a cooling of the hydrothermal fluid of
519 about 70 °C in 300-400 ka. Therefore, while the Castelnuovo dell'Abate travertines were strictly
520 and directly connected with the Mt. Amiata geothermal anomaly, the Semproniano system, which is
521 located about 20 km to the south, was influenced not only by the Mt. Amiata geothermal anomaly,
522 but also by further paleoenvironmental and/or paleoclimate factors (see below).

523 The Sr- and Nd-isotopes as well as the REE patterns help to characterize the origin of the
524 hydrothermal fluids. The rather homogeneous Sr- and Nd-isotope values are indicative of a unique
525 reservoir for the deposition of travertines and calcite veins. Sr- and Nd- isotope values are different
526 from isotopic signature of Mt. Amiata volcanic rocks (Conticelli et al. 2015). In particular, our Sr-
527 isotope values are in the range of those obtained for the Mesozoic sedimentary units of central Italy
528 (e.g., Barbieri et al., 1979; Cortecci and Lupi, 1994; Barbieri and Morotti, 2003; Gasparrini et al.,
529 2013) and for the hydrothermal springs of Saturnia (Barbagli et al., 2013). This suggests no
530 contamination through volcanic units during underground circulation of these fluids. This
531 interpretation is compatible with the REE patterns that are similar to those obtained from the
532 Tuscan Nappe limestone from the Larderello-Travale geothermal area (Möller et al., 2003; Fig. 9).
533 Accordingly, we consider the Mesozoic limestones of the Albegna area (e.g., Bonciani et al., 2005;
534 Brogi, 2008; Guastaldi et al., 2014) as the main reservoir of the hydrothermal system and the
535 probable source for the chemical signature of the studied carbonates. Eventually, the best scenario
536 explaining the entire hydrothermal fluid circuit should involve variable mixing of meteoric waters
537 with fluids characterized by water-rock isotopic exchange similar to the broad field of endogeneous
538 fluids (e.g., Crossey et al., 2009).

4.4. Estimation of CO_2 outflow

Minimum value of total CO_2 volume leaked during the formation of the Semproniano giant vein can be estimated from the volume of $CaCO_3$ precipitated (Crossey et al., 2009; Frery, 2012; Karlstrom, 2013). It has been shown that the volume of leaked CO_2 precipitated in travertine/vein deposits is only a minor part of the total leakage, representing between 6.6% and 10% (Shipton et al., 2005) of the total dissolved CO_2. According to Frery (2012), it is possible to calculate only the minimum value of CO_2 leakage during $CaCO_3$ vein formation for two reasons: (i) the proportion between precipitated CO_2 and total leaked CO_2 includes only the dissolved part of the CO_2 at the surface, thus disregarding the CO_2 escaping as free phase (i.e., degassing); (ii) after formation, the vein or travertine deposit may have undergone erosional processes, which are difficult to accurately quantify.

For fossil travertines or $CaCO_3$ veins, the total mass of precipitated CO_2 ($m_{CO2}^{precipitated}$) can be calculated using the calcium carbonate precipitation equation:

$$m_{CO2}^{precipitated} = \rho_{CaCO3} \cdot V_{CaCO3}\{M_{CO2}|M_{CaCO3}\} \qquad \text{(Eq. 1)}$$

where ρ_{CaCO3} and$\{M_{CO2}|M_{CaCO3}\}$ are considered as constant parameters: ρ_{CaCO3}= $2.7 \cdot 10^3$ kg/m^3; M_{CO2} = 44g/mol, and M_{CaCO3} = 100.1 g/mol.

Based on field observations, we estimate the volume of the Semproniano giant vein assuming a length of 500 m and a width of 50 m. for the thickness of the vein, we consider two alternative end members: 10 m (the observable vein exposed in the field), and 50 m (estimated through geological cross-sectioning; Fig. 2b). For a thickness of 10 m, the estimated total mass of CO_2 leakage are 3 x 10^6 and 5 x 10^6 tons, for total dissolved CO_2 masses of 10 and 6.6%, respectively. For a depth of 50 m 14 x 10^6 and 22 x 10^6 tons are calculated. Collectively, all these values provide a CO_2 leakage between 5 ton/a and 37 tons/a over the 600 ka longevity of the Semproniano giant vein, corresponding to a CO_2 flux between 5 x 10^6 mol a^{-1} km^{-2} and 3 x 10^7 mol a^{-1} km^{-2}. These estimates

564 are of the same order of magnitude of measured average CO_2 flux discharged by present-day
565 thermal springs in central Italy (between 1×10^4 mol a^{-1} km^{-2} and 5×10^7 mol a^{-1} km^{-2}, Minissale,
566 2004; Frondini et al., 2008) and it is two order of magnitude lower than the CO_2 flux (3.7×10^9 mol
567 a^{-1}) in present-day thermal springs on the Colorado Plateau, USA (Crossey et al., 2009). For
568 comparison, the estimated CO_2 flux during the formation of the Semproniano giant vein is about
569 four order of magnitude lower than the deeply sourced (endogenic) CO_2 in non-volcanic areas of
570 Italy (10^{11} mol a^{-1}, Rogie et al., 2000) and represent about one millionth of the present-day CO_2
571 released from volcanic areas at the global scale (Gerlach, 2011).
572
573 ***4.5. Paleoclimate influence***
574 To determine a possible influence of paleoclimate on the growth of the Semproniano giant vein,
575 in Fig. 11 we matched our U/Th ages (Tables 2 and S1) with Quaternary glacial cycles, using the
576 curve extracted from the deep sea oxygen isotope trend elaborated by Zachos et al. (2001), and the
577 pollen record of the Valle di Castiglione, located about 150 km to the south of the study area (Fig.
578 1a), elaborated by Tzedakis et al. (2001).
579 We note that, except for two points, most samples from the giant vein fall within the inter-glacial
580 stages. Also the host rock of the giant vein and the bedded travertine on the vein flanks match well
581 with interglacial stages (Fig. 11). It is noteworthy that six samples fall within marine isotope stages
582 MIS 5 and MIS 7, which are suggested to be humid times by the pollen curve (Fig. 11).
583 The darting, thus suggests that the Semproniano giant vein formed preferentially during warm
584 and humid climate periods characterized by high stands of the water table promoting a greater fluid
585 discharge. Similar patterns have been suggested for other Quaternary travertine deposits (e.g.,
586 Dramis et al., 1999; Frank et al., 2000; Rihs et al., 2000; Soligo et al., 2002; Pentecost, 2005; Luque
587 and Julià, 2007; Faccenna et al., 2008; Kampman et al., 2012; Priewisch et al. 2014).

588 This scenario is different from the one proposed by Uysal et al. (2007, 2009) for banded
589 travertines precipitated in co-seismic fissures of the Denizli basin (Turkey) which was based on
590 U/Th ages and REE data. These authors, proposed that carbonate precipitation was controlled by
591 seismic-related CO_2 exsolution from a depressed water table during glacial stages. Ages obtained
592 for Turkish travertines by Özkul et al., (2013) and Toker et al., (2015) show that deposition was
593 active during glacial and interglacial time, indicating that travertine precipitation during late
594 Quaternary was not strongly influenced by climatic variation. In particular, we found similarities
595 with Toker et al., (2015) whose recognized that the highest amount travertine precipitation in
596 Kocabas (Denizli basin, Turkey) occurred during MIS 5 (interglacial) and proposed that active fault
597 systems favored the rise of hydrothermal fluids and travertine deposition,
598 Finally, our results for the Semproniano giant vein suggest that high stand of the water table was
599 a primary influencing factor in the vein formation.
600
601 ***4.6. Relationships between the giant vein and nearby travertine deposits: the fluid circuit***
602 The Poggio Semproniano and Poggio I Piani travertine plateaus constitute the largest travertine
603 deposits in the Semproniano area (Fig. 3a). Although the dataset for these deposits is smaller than
604 that of the giant vein, the C- and O-isotope values are comparable (Fig. 8b), showing that the
605 hydrothermal parental fluids were very similar. The Sr-, Nd-isotopes, and REE data (Table 4 and
606 Fig. 9) confirm that the parental fluid circuit and reservoir was mainly the Mesozoic limestones of
607 the Albegna basin.
608 U/Th ages for the bedded travertine samples from the plateaus (Table 2), 171 ± 14 ka for Poggio
609 Semproniano, 198 ± 18 ka for Poggio I Piani) indicate that the formation of the two plateaus was at
610 least in part contemporaneous with that of the Semproniano giant vein. Moreover, also the activity
611 of the nearby Mt. Amiata volcanic district (300-190 ka, Cadoux and Pinti, 2009; 300-225 ka,
612 Laurenzi et al., 2015) was partly contemporaneous with the $CaCO_3$ mineralizations of the

613 Semproniano area, with the giant vein being partly older and partly younger than the volcanic
614 district.

615 From previous studies we know that while fissure ridges such as the Semproniano giant vein are
616 aggradational systems that tend to grow vertically due to the scarcity of feeding fluids (i.e., $CaCO_3$
617 precipitates contributing to the vertical grow of the deposit), travertine plateaus are progradational
618 systems where the abundance of feeding fluids contribute to the horizontal grow (progradation) of
619 the deposit (Faccenna et al., 2008; De Filippis et al. 2013a). We also know that fissure ridges and
620 plateaus can coexist, in space and time, in geothermal areas where the abundance of geothermal
621 fluids primarily feeds the plateau whereas the fissure ridge(s) constitutes a remote apophysis of the
622 plateau with a scarcity of fluids that provokes the aggradation development of the fissure ridge (e.g.,
623 Tivoli travertines; De Filippis et al., 2013b).

624 The possible scenario for the genesis of the Semproniano giant travertine vein is a structurally-
625 controlled pathway (faults and fractures) for the circulating mineralising fluids during the
626 Quaternary. Dominant meteoric fluids interacted with the carbonate reservoir of the Mt. Amiata
627 volcano and were heated at depth, where the heat source is maintained by the regional geothermal
628 anomaly (Fig. 12a). In this scenario, the Semproniano giant vein resulted as an epithermal fluid
629 discharge area after convective circulation of the CO_2-enriched hydrothermal fluids (Fig. 12b). In
630 particular, we can assume a fluid pressure cycling in a long-lived fault-valve behavior setting (Cox
631 et al., 2001; Sibson, 2004; Cox, 2010), assisted by fracture network generation and maintenance
632 that could have been provided by the well-known N-S-striking fault zone system active during
633 Quaternary time in the Mt Amiata-Albegna basin region (Zanchi and Tozzi, 1987; Brogi, 2004b;
634 Bellani et al., 2004; Brogi and Fabbrini, 2009). In this model, the Semproniano giant vein (i.e., the
635 fissure ridge) is interpreted as an apophysis of a large geothermal field characterized by the
636 deposition of big travertine plateaus.

637

638 **Conclusions**

(1) The thickest continuous vein hitherto documented in the literature (50 m) is found and studied within a fissure ridge travertine exposed in the Semproniano village, in the hydrothermal area surrounding the Pleistocene Mt. Amiata volcano in southern Tuscany, Italy.

(2) The thickness of the Semproniano vein is connected with its probable shallow emplacement and with the unusual longevity of the hydrothermal activity between at least 650 and 85 ka.

(3) The epithermal fluid supply feeding the Semproniano giant vein is not directly connected with the main volcanic paroxysmal activity of the Mt. Amiata volcano (which is younger than the early growth of the vein), rather with the positive geothermal anomaly associated with its pre-eruptive stages (Cadoux et al., 2009) through structurally-controlled fluid pathways which created and maintained active convection and supply of CO_2-enriched meteoric fluids.

(5) The growth of the Semproniano giant vein was modulated by by Pleistocene climate oscillations, with warm humid interglacial periods being the preferential phases of vein accretion, due to the higher fluid discharge.

(6) Structures such as the Semproniano giant vein can be used to estimate the long-term release of CO_2 from geothermal/volcanic provinces, thus improving our knowledge of the CO_2 cycle on Earth.

Aknowledgements

The authors thank C. Faccenna for fruitful discussions, G. Fellini for her help in the field and in the lab at ETH Zurich, and M. Brilli for isotope analysis of sample SP16. The "Saturnia Travertini" company is acknowledged for providing us any logistic assistance. The "Terme di Saturnia SPA & Golf Resort" is acknowledged for providing us any logistic assistance. U/Th dating at the HISPEC was supported by the Taiwan ROC MOST grants (103-2119-M-002-022 and 104-2119-M-002-003 to CCS). S.K. was supported by the János Bolyai scholarship of the Hungarian Academy of Sciences and the Hungarian Scientific Research Fund (OTKA 101664).

665 **References**

666 Altunel E., Hancock P.L., 1993a. Active fissuring and faulting in Quaternary travertines at
667 Pamukkale, western Turkey. In: Stewart, I.S., Vita-Finzi, C., Owen, L.A. (Eds.), Neotectonics
668 and Active Faulting: Zeitschrift fuer Geomorphologie Supplement, 94, 285–302.
669 Altunel E., Hancock P.L., 1993b. Morphology and structural setting of Quaternary travertines at
670 Pamukkale, Turkey. Geological Journal, 28, 335–346.
671 Altunel E., Hancock P.L., 1996. Structural attributes of travertine-filled extensional fissures in the
672 Pamukkale plateau, western Turkey. International Geology Review, 38, 768–777.
673 Altunel E., Karabacak V., 2005. Determination of horizontal extension from fissure-ridge
674 travertines: a case study from the Denizli Basin, southwestern Turkey. Geodinamica Acta, 18,
675 333–342.
676 Annunziatellis A., Beaubien S.E., Bigi S., Ciotoli G., Coltella M., Lombardi S., 2008. Gas
677 migration along fault systems and through the vadose zone in the Latera caldera (central
678 Italy): implications for CO2 geological storage. International Journal of Greenhouse Gas
679 Control, 2, 353-372.
680 Barbagli A., Brogna F.N.A., Callegari I., Guastaldi E., Liali G., Marsico N., Rezza C., Trotta M.,
681 2013. Approccio multi-isotopico ed idrogeochimico per la caratterizzazione di acque termali:
682 il caso di Saturnia (GR). Italian Journal of Groundwater, AS07029, 025-040, DOI
683 10.7343/AS-049-13-0076.
684 Barberi F., Buonasorte G., Cioni R., Fiordelisi A., Foresi L., Iaccarino S., Laurenzi M.A., Sbrana A.,
685 Vernia L., Villa I.M., 1994. Plio-Pleistocene geological evolution of the geothermal area of
686 Tuscany and Latium. Memorie Descrittive della Carta Geologica d'Italia, 49, 77–133.
687 Barbieri M. and Morotti M., 2003. Hydrogeochemistry and strontium isotopes of spring and mineral
688 waters from Monte Vulture volcano, Italy. Applied Geochemistry, 18, 117-125.
689 Barbieri M., Masi U., Tolomeo L., 1979. Origin and distribution of strontium in the travertines of
690 Latium (central Italy). Chemical Geology, 24, 181-188.

691 Barchi M., Minelli G., Pialli G., 1998. The CROP-03 profile: a synthesis of results on deep
692 structures of the Northern Apennines. Memorie della Società Geologica Italiana, 52, 383-400.
693 Batini F., Brogi A., Lazzarotto A., Liotta D., Pandeli E. 2003. Geological features of the
694 Larderello–Travale and Monte Amiata geothermal areas (southern Tuscany, Italy). Episodes,
695 26, 239-244.
696 Beasley C.J., Fiduk J.C., Bize E., Boyd A., Frydman M., Zerilli A., Dribus J.R., Moreira J.L.P.,
697 Capeliero Pinto A.C., 2010: Brazil's subsalt play. Oilfield Review, 22, No. 3, 28-37.
698 Bellani S., Brogi A., Lazzarotto A., Liotta D., Ranalli G., 2004. Heat flow, deep temperatures and
699 extensional structures in the Larderello geothermal field (Italy). Constraints on geothermal
700 fluid flow. Journal of Volcanology and Geothermal Research, 132, 15–29.
701 Bickle M., Kampman N., 2013. Lessons in carbon storage from geological analogues. Geology, 41,
702 525-526.
703 Billi A., Tiberti M.M., Cavinato G.P., Cosentino D., Di Luzio E., Keller J.V.A., Kluth C., Orlando
704 L., Parotto M., Praturlon A., Romanelli M., Storti F., Wardell N., 2006. First results from the
705 CROP-11 deep seismic profile, central Apennines, Italy: evidence of mid-crustal folding.
706 Journal of Geological Society London, 163, 583-586.
707 Billi A., Valle A., Brilli M., Faccenna C., Funiciello R., 2007. Fracture-controlled fluid circulation
708 and dissolutional weathering in sinkhole-prone carbonate rocks from central Italy. Journal of
709 Structural Geology, 29, 385-395.
710 Bodnar R.J., Vytik M.O., 1994. Interpretation of microthermometric data for H_2O–NaCl fluid
711 inclusions. In: De Vivo B., Frezzotti M.L. (eds) Fluid inclusions in minerals: methods and
712 applications. Virginia Polytechnic Institute, Blacksburg, 117-130.
713 Bodnar R.J., 2003. Reequilibration of fluid inclusions In: Samson IM, Anderson AJ, Marshall DD
714 (eds) Fluid Inclusions: Analysis and Interpretation. Mineralogical Association of Canada,
715 Short Course, 32, 213-230.

716 Bonazzi U., Fazzini P., Gasperi G., 1992. Note alla carta geologica del Bacino del Fiume Albegna.
717 Bollettino della Società Geologica Italiana, 111, 341-354.
718 Bonciani F., Callegari I., Conti P., Cornamusini G., Carmignani L., 2005. Neogene post-collisional
719 evolution of the internal Northern Apennines: insights from the upper Fiora and Albegna
720 valleys (Mt. Amiata geothermal area, southern Tuscany). Bollettino della Società Geologica
721 Italiana, Special Volume 3, 103-118.
722 Bons P.D., 2001. The formation of large quartz veins by rapid ascent of fluids in mobile
723 hydrofractures. Tectonophysics, 336, 1-17.
724 Bons P.D., Elburg M.A., Gomez-Rivas, E., 2012. A review of the formation of tectonic veins and
725 their microstructures. Journal of Structural Geology, 43, 33-62
726 Bosi C., Messina P., Rosati M., Sposato A., 1996. Età dei travertini della Toscana meridionale e
727 relative implicazioni neotettoniche. Memorie della Società Geologica Italiana, 51, 293-304.
728 Bossio A., Foresi L.M., Mazzei R., Salvatorini G., Sandrelli F., Bilotti M., Colli A., Rossetto R.,
729 2004. Geology and stratigraphy of the southern sector of the Neogene Albegna River Basin
730 (Grosseto, Tuscany, Italy): Geologica Romana, 37, 165-173.
731 Bottinga Y., 1968. Calculation of fractionation factors for carbon and oxygen isotopic exchange in
732 the system calcite–carbon dioxide–water. Journal of Physical Chemistry, 72, 800–808
733 Breitenbach S.F:M. and Bernasconi S.M. 2011. Carbon and oxygen isotope analysis of small
734 carbonate samples (20 to 100 µg) with a GasBench II preparation device. Rapid
735 Communications in Mass Spectrometry, 25, 1910-1914.
736 Brogi, A., 2004a. Faults linkage, damage rocks and hydrothermal fluid circulation: tectonic
737 interpretation of the Rapolano Terme travertines (southern Tuscany, Italy) in the context of
738 the Northern Apennines Neogene–Quaternary extension. Eclogae Geologicae Helvetiae, 97,
739 307–320.

740 Brogi A., 2004b. Miocene extension in the inner Northern Apennines: the Tuscan Nappe
741 megaboudins in the Mt. Amiata geothermal area and their influence on Neogene
742 sedimentation. Bollettino della Società Geologica Italiana, 123, 513-529.
743 Brogi A., 2008. The structure of the Monte Amiata volcano-geothermal area (Northern Apennines,
744 Italy): Neogene-Quaternary compression versus extension. International Journal of Earth
745 Sciences, 97, 677-703. DOI 10.1007/s00531-007-0191-1
746 Brogi A., Liotta, D., 2008. Highly extended terrains, lateral segmentation of the substratum, and
747 basin development: the Middle–Late Miocene Radicondoli Basin (inner northern Apennines,
748 Italy). Tectonics, 27, TC 5002.
749 Brogi A., Fabbrini L, 2009. Extensional and strike-slip tectonics across the Monte Amiata–Monte
750 Cetona transect (Northern Apennines, Italy) and seismotectonic implications. Tectonophysics,
751 476, 195-209.
752 Brogi A., Capezzuoli E., 2009. Travertine deposition and faulting: the fault-related travertine
753 fissure-ridge at Terme S. Giovanni, Rapolano Terme (Italy). International Journal of Earth
754 Sciences (Geologische Rundschau), 98, 931–947.
755 Brogi A., Capezzuoli E., Ague R., Branca M., Voltaggio M., 2010. Studying travertines for
756 neotectonics investigations: middle–late Pleistocene syn-tectonic travertine deposition at Serre
757 di Rapolano (Northern Apennines, Italy). International Journal of Earth Sciences, 99, 1382–
758 1398.
759 Brogi A., 2011. Bowl-shaped basin related to low-angle detachment during continental extension:
760 The case of the controversial Neogene Siena Basin (central Italy, Northern Apennines).
761 Tectonophysics, 499, 54-76.
762 Brogi A., Capezzuoli E., Buracchi E., Branca M., 2012. Tectonic control on travertine and
763 calcareous tufa deposition in a low-temperature geothermal system (Sarteano, Central Italy).
764 Journal of the Geological Society, 169, 461–476.

765 Brogi A., Fidolini F., Liotta D., 2013. Tectonic and sedimentary evolution of the Upper Valdarno
766 Basin: new insights from the lacustrine S. Barbara Basin. Italian Journal of Geosciences,
767 132/1, 81-97.
768 Brogi A., Capezzuoli E., Martini I., Picozzi M., Sandrelli F., 2014. Late Quaternary tectonics in the
769 inner Northern Apennines (Siena Basin, southern Tuscany, Italy) and their seismotectonic
770 implication. Journal of Geodynamics, 76, 25-45.
771 Brogi A., Capezzuoli, E., Liotta D., Meccheri M., 2015. The Tuscan Nappe structures in the Monte
772 Amiata geothermal area (central Italy): a review. Italian Journal of Geosciences, 134-2, 219-
773 236.
774 Buonasorte G., Cataldi R., Ceccarelli A., Costantini A., D'Offizi S., Lazzarotto A., Ridolfi A.,
775 Baldi P., Barelli A., Bertini G., Bertrami R., Calamai A., Cameli G., Corsi R., D'Acquino C.,
776 Fiordelisi A., Gezzo A. & Lovari F., 1988. Ricerca ed esplorazione nell'area geotermica di
777 Torre Alfina (Lazio – Umbria). Bollettino della Società Geologica Italiana, 107, 265-337.
778 Burnside, N.M., Shipton, Z.K., Dockrill, B., Ellam, R.M., 2013. Man-made versus natural CO2
779 leakage: A 400 k.y. history of an analogue for engineered geological storage of CO2: Geology,
780 41, 471–474.
781 Cadoux A., Pinti D.L., 2009. Hybrid character and pre-eruptive events of Mt Amiata volcano (Italy)
782 inferred from geochronological, petro-geochemical and isotopic data. Journal of Volcanology
783 and Geothermal Research, 179, 169-190.
784 Çakır Z., 1999. Along-strike discontinuity of active normal faults and its influence on Quaternary
785 travertine deposition; examples from western Turkey. Turkish Journal of Earth Sciences, 8,
786 67–80.
787 Calvo P. and Regueiro M., 2010. Carbonate rocks in the Mediterranean region, from classical to
788 innovative uses of building stone. Geological Society, London, Special Publication, 331, 27-
789 35.

790 Capezzuoli E., Ruggieri G., Brogi A., Liotta D., 2013. Fluid inclusion analyses in hydrothermal
791 veins associated to travertine: insights from the Semproniano fissure-ridge type travertine
792 deposits (southern Tuscany, Italy). Fist Geoitalia 2013, IX Forum di Scienze della Terra, Pisa
793 16-18 Settembre 2013.
794 Carmignani L., Decandia F.A., Fantozzi P.L., Lazzarotto A., Liotta D. & Meccheri M., 1994.
795 Tertiary extensional tectonics in Tuscany (Northern Apennines, Italy). Tectonophysics, 238,
796 295-315.
797 Carmignani L., Conti P., Cornamusini G., Pirro A. 2013. Geological map of Tuscany (Italy).
798 Journal of Maps, 9:4, 487-497, DOI:10.1080/17445647.2013.820154
799 Cavinato G.P., De Celles P.G., 1999. Extensional basins in the tectonically bimodal central
800 Apennines fold-thrust belt, Italy: response to corner flow above a subducting slab in
801 retrograde motion. Geology, 27, 955-958.
802 Chafetz H.S., Folk R.L., 1984. Travertines: depositional morphology and the bacterially constructed
803 constituents. Journal of Sedimentary Petrology, 54, 289–316.
804 Chiarabba C., Amato A., Fiordelisi A., 1995. Upper crustal tomographic images of the Amiata–
805 Vulsini geothermal region, central Italy. Journal of Geophysical Research, 100, 4053–4066.
806 Cipollari P., Cosentino D., 1995. Miocene unconformities in the Central Apennines: geodynamic
807 significance and sedimentary basin evolution. Tectonophysics, 252, 375-389.
808 Collettini C., De Paola N., Holdsworth R.E., Barchi M.R., 2006. The development and behavior of
809 low-angle normal faults during Cenozoic asymmetric extension in the Northern Apennines,
810 Italy. Journal of Structural Geology, 28, 333-352.
811 Cortecci G., Lupi L., 1994. Carbon, oxygen and strontium isotope geochemistry of carbonate rocks
812 from the Tuscan Nappe, Italy. Mineralogia et Petrographica acta, 37, 63-80.
813 Cox S.F., Knackstedt M.A., Braun J., 2001. Principles of structural controls on permeability and
814 fluid flow in hydrothermal systems. Reviews in Economic Geology, 14, 1–24.

Cox S.F., 2010. The application of failure mode diagrams for exploring the roles of fluid pressure and stress states in controlling styles of fracture-controlled permeability enhancement in faults and shear zones. Geofluids, 10, 217–233.

Crossey L.J., Fischer T.P., Patchett P.J., Karlstrom K.E., Hilton D.R., Newell D.L., Huntoon P., Reynolds A.C., de Leeuw G.A.M., 2006. Dissected hydrologic system at the Grand Canyon: interaction between deeply derived fluids and plateau aquifer waters in modern springs and travertine. Geology, 34, 25-28.

Crossey L.J., Karlstrom K.E., Springer A.E., Newell D., Hilton D.R., Fischer T., 2009. Colorado Plateau region - Neotectonic connections and implications for groundwater systems. Geological Society of America Bulletin, 121 (7/8), 1034-1053.

Crossey L.C., Karlstrom K.E., Dorsey R., Pearce J., Wan E., Beard L.S., Asmerom Y., Polyak., Crow R.S., Cohen A., Bright J., Pecha, M.E, 2015. Importance of groundwater in propagating downward integration of the 6-5 Ma Colorado River system: Geochemistry of springs, travertines and lacustrine carbonates of the Grand Canyon region over the past 12 Ma. Geosphere, 11, 3, 1-23.

De Filippis L., Billi A., 2012. Morphotectonics of fissure ridge travertines from geothermal areas of Mammoth Hot Springs (Wyoming) and Bridgeport (California). Tectonophysics, 548-549, 34-38.

De Filippis L., Faccenna C., Billi A., Anzalone E., Brilli M., Özkul M., Soligo M., Tuccimei P., Villa I.M., 2012. Growth of fissure ridge travertines from geothermal springs of Denizli basin, western Turkey. Geological Society of America Bulletin, 124, 1629–1645.

De Filippis L., Faccenna C., Billi A., Anzalone E., Brilli M., Soligo M., Tuccimei P., 2013a. Plateau versus fissure ridge travertines from Quaternary geothermal springs of Italy and Turkey: Interactions and feedbacks between fluid discharge, paleoclimate, and tectonics. Earth-Science Reviews, 123, 35-52.

De Filippis L., Anzalone E., Billi A., Faccenna C., Poncia P.P., Sella P., 2013b. The origin and growth of a recently-active fissure ridge travertine over a seismic fault, Tivoli, Italy. Geomorphology, 195, 13-26.

Dewey J.F., 1988. Extensional collapse of orogens. Tectonics, 7, 1123-1139.

DePaolo D.J., Wasserburg G.J., 1976. Nd isotopic variations and petrogenetic models. Geophysical Research Letters, 3, 249–252.

Diamond L. W., 2003. Systematics of H2O inclusions. In: Samson IM, Anderson AJ, Marshall DD (eds.) Fluid inclusions: analysis and interpretation. Mineralogical Association of Canada, Short Course, 32, 55–80.

Dini A., Granelli G., Puxeddu M., Ruggirei G., 2005. Origin and evolution of Pliocene–Pleistocene granites from the Larderello geothermal field (Tuscan Magmatic Province, Italy). Lithos, 81, 1-31.

Dramis F., Materazzi M., Cilla G., 1999. Influence of climatic changes on freshwater travertine deposition: A new hypothesis. Physics and Chemistry of the Earth, Part A: Solid Earth and Geodesy, 24, 893-897, doi: 1127 10.1016/S1464-1895(99)00132-5.

Ederfield H., Greaves M.J., 1982. The rare-elements in seawater. Nature, 296, 214–219.

Edwards R.L., Chen J.H., Wasserburg, G.J., 1988. ^{238}U–^{234}U–^{230}Th systematics and the precise measurement of time over the last 500,000 years. Earth and Planetary Science Letters, 81, 175–192.

El Desouky H., Soete J., Claes H., Özkul M., Vanhaecke F., Swennen R., 2015. Novel applications of fluid inclusions and isotope geochemistry in unravelling the genesis of fossil travertine systems. Sedimentology, 62, 27-57.

Faccenna C., Soligo M., Billi A., De Filippis L., Funiciello R., Rossetti C., Tuccimei P., 2008. Late Pleistocene depositional cycles of the Lapis Tiburtinus travertine (Tivoli, central Italy): possible influence of climate and fault activity. Global and Planetary Change, 63, 299–308.

865 Ford T.D., Pedley H.M., 1996. A review of tufa and travertine deposits of the world. Earth-Science
866 Reviews 41, 117–175.
867 Frank N., Braum M., Hambach U., Mangini A., Wagner G., 2000. Warm period growth of
868 travertine during the last 1150 interglaciation in Southern Germany. Quaternary Research, 54,
869 38–48. doi:10.1006/qres.2000.2135.
870 Frery E., 2012. Episodic circulation of reactive fluids along faults. From travertine- to basin-scale
871 based on the Colorado Plateau natural example (USA). PhD Thesis, Université Joseph
872 Fourrier Grenoble (France), 247pp.
873 Frery E., Gratier J.P., Ellouz-Zimmerman N., Loiselet C., Braun J., Deschamps P., Blamart D.,
874 Hamelin B., Swennen R., 2015. Evolution of fault permeability during episodic fluid
875 circulation: Evidence for the effects of fluid–rock interactions from travertine studies (Utah–
876 USA). Tectonophysics, http://dx.doi.org/10.1016/j.tecto.2015.03.018.
877 Frondini F., Caliro S., Cardellini C., Chiodini G., Morgantini N., Parello F., 2008. Carbon dioxide
878 degassing from Tuscany and Northern Latium (Italy). Global and Planetary Change 61, 89–
879 102.
880 Gandin A. and Capezzuoli E., 2008. Travertine versus Calcareous tufa: distinctive petrologic
881 features and related stable isotopes signature. Il Quaternario Italian Journal of Quaternary
882 Science, 21, 125-136.
883 Gerlach T., 2011. Volcanic versus anthropogenic carbon dioxide. Eos, 92 no. 24, 201-202.
884 Gianelli G., Manzella A., Puxeddu M., 1997. Crustal models of southern Tuscany (Italy).
885 Tectonophysics, 281, 221–239.
886 Gibert R.O., Taberner C., Sáez A., Giralt S., Alonso R.N., Edwards R.L., Pueyo J.J., 2009. Igneous
887 origin of CO_2 in ancient and recent hot-spring waters and travertines from the northern
888 Argentinean Andes. Journal of Sedimentary Research, 79, 554-567.
889 Goldtsein R.H., Reynolds T.J., 1994. Fluid inclusion microthermometry. In: Systematics of fluid
890 inclusions in diagenetic minerals. Society for Sedimentation Geology, short course 31, 7-121.

891 Gonfiantini R., Panichi C., Tongiorgi E., 1968. Isotopic disequilibrium in travertine deposition.
892 Earth and Planetary Science Letters, 5, 55-58.
893 Gradziński M., Wróblewski W., Duliński M., Hercman H., 2014. Earthquake-affected development
894 of a travertine ridge. Sedimentology, 61, 238–263.
895 Gratier, J. P., Frery, E., Deschamps, P., Røyne, A., Renard, F., Dysthe, D., Ellouz-Zimmerman, N.,
896 Hamelin, B., 2012. How travertine veins grow from top to bottom and lift the rocks above
897 them: the effect of crystallization force. Geology, 40, 1015–1018.
898 Guastaldi E., Graziano L., Liali G., Nunzio F., Brogna A., Barbagli A., 2014. Intrinsic vulnerability
899 assessment of Saturnia thermal aquifer by means of three parametric methods: SINTACS,
900 GODS and COP. Environmental Earth Sciences, DOI 10.1007/s12665-014-3191-z.
901 Guo L., Andrews J., Riding R., Dennis P., Dresser, Q., 1996. Possible microbial effects on stable
902 carbon isotopes in hot travertine. Journal of Sedimentary Research, 66, 468-473.
903 Guo L. and Riding R., 1999. Rapid facies changes in Holocene fissure ridge hot spring travertines,
904 Rapolano Terme, Italy. Sedimentology, 46, 1145-1158. doi:10.1046/j.1365-
905 3091.1999.00269.x
906 Hancock P.L., Chalmers R.M.L., Altunel E., Çakir Z., 1999. Travitonics: using travertine in active
907 fault studies. Journal of Structural Geology, 21, 903–916.
908 Jolivet L., Faccenna C., Goffé B., Mattei M., Rossetti F., Brunet C., et al., 1998. Midcrustal shear
909 zones in post-orogenic extension: example from the northern Tyrrhenian Sea (Italy). Journal
910 of Geophysical Research, 103, 12123–12160.
911 Kampman N., Burnside N.M., Shipton Z.K., Chapman H.J., Nicholl J.A., Ellam R.M., Bickle M.J.,
912 2012. Pulses of carbon dioxide emissions from intracrustal faults following climatic warming.
913 Nature Geoscience, 5, 352-358.
914 Karlstrom K.E., Crossey L.J., Hilton D.R., Barry P.H., 2013.Mantle ^{3}He and CO_2 degassing in
915 carbonic and geothermal springs of Colorado and implications for neotectonics of the Rocky
916 Mountains. Geology, 41, 495-498.

917 Kele S., Özkul M., Fórizs I., Gökgöz A., Baykara M.O., Alçiçek M.C., Németh T., 2011. Stable
918 isotope geochemical study of Pamukkale travertines: new evidences of lowtemperature non-
919 equilibrium calcite-water fractionation. Sedimentary Geology, 238, 191–212.
920 Kele S., Breitenbach S.F.M., Capezzuoli E., Meckler A.N., Ziegler M., Millan I.M., Kluge T., Deák
921 J., Hanselmann K., John C., Yan H., Liu Z., Bernasconi S.M., 2015. Temperature dependence
922 of oxygen- and clumped isotope fractionation in carbonates: a study of travertines and tufas in
923 the 6-95°C temperature range. Geochimica et Cosmochimica Acta, 168, 172-192.
924 Keller J.V.A., Minelli G., Pialli G., 1994. Anatomy of a late orogenic extension: the Northern
925 Apennines case. Tectonophysics, 238, 275–294.
926 Laurenzi M.A., Braschi E., Casalini M., Conticelli S., 2015. New $^{40}Ar/^{39}Ar$ dating and revision of
927 geochronology of the Monte Amiata Volcano, Central Italy. Italian Journal of Geosciences,
928 134-2, 255-265.
929 Liotta D., 1994. Structural features of the Radicofani basin along the Piancastagnaio (Mt. Amiata) -
930 S. Casciano dei Bagni (Mt. Cetona) cross section. Memorie della Società Geologica, Italiana
931 48, 401–408.
932 Liotta, D., Ruggieri, G., Brogi, A., Fulignati, P., Dini, A., Cardini, I., 2010. Migration of
933 geothermal fluids in extensional terrains: the ore deposits of the Boccheggiano-Montieri area
934 (southern Tuscany, Italy). International Journal of Earth Sciences, 99, 623–644
935 Locardi E., Nicolich R., 1988. Geodinamica del Tirreno e dell'Appennino centro-meridionale: la
936 nuova carta della Moho (Geodynamic of the Thyrrenian Sea and of Central-Southern
937 Apennine: the new map of Moho). Memorie della Societa Geologica Italiana, 41, 121–140.
938 Ludwig K.R., 2003. Isoplot/Ex version 3.00, A Geochronological Toolkit for Microsoft Excel.
939 Berkeley Geochronology Center Special Publication, 4.
940 Luque J.A. and Julià R., 2007. U/Th dating of Quaternary travertines at the middle River Llobregat
941 (NE Iberian 1232 Peninsula, Northwestern Mediterranean). Correlation with sea-level changes.
942 Geologica Acta, 5, 109-117.

943 Maggi M., Cianfarra P., Salvini F., de Lima C.C., 2015. Staircase fractures in microbialites and the
944 role of lamination-related mechanical anisotropy: the example of the Acquasanta Terme
945 travertine deposits (central Italy). Geological Society of America Bullettin, 127, no. 5-6, 879-
946 896.
947 Malinverno A., Ryan W., 1986. Extension in the Tyrrhenian sea and shortening in the Apennines as
948 result of arc migration driven by sinking of the lithosphere. Tectonics, 5, 227-245.
949 Marroni M., Moratti G., Costantini A., Conticelli S., Benvenuti M.G., Pandolfi L., Bonini M.,
950 Cornamusini G., Laurenzi M.A., 2015. Geology of the Monte Amiata region, Southern
951 Tuscany, Central Italy. Italian Journal of Geosciences, 134-2, 171-199.
952 Martelli L., Moratti G., Sani F., 1989. Analisi strutturale dei travertini della Toscana meridionale
953 (Valle dell'Albegna). Bollettino della Società Geologica Italiana, 108, 197-205.
954 Martini I.P., Sagri M., 1993. Tectono-sedimentary characteristics of Late Miocene –Quaternary
955 extensional basins of the northern Apennines, Italy. Earth Science Reviews, 34, 197 – 233
956 Massoli D., Koyi H.A., Barchi M.R., 2006. Structural evolution of a fold and thrust belt generated
957 by multiple décollements: Analogue models and natural examples from the Northern
958 Apennines (Italy). Journal of Structural Geology, 28, 185-199.
959 McLennan S.M., 1989. Rare earth elements in sedimentary rocks. Influence of provenance and
960 sedimentary processes. In: Lipin, B.R., McKay, G.A. (Eds.), Geochemistry and Mineralogy of
961 Rare Earth Elements. Reviews in Mineralogy, 21. Mineralogical Soc. America, Washington,
962 pp. 169–200.
963 Mesci L.B., Gürsoy H., Tatar O., 2008. The evolution of travertine masses in the Sivas area (central
964 Turkey) and their relationships to active tectonics: Turkish Journal of Earth Sciences, 17, 219–
965 240.
966 Minissale A., 2004. Origin, transport and discharge of CO2 in central Italy. Earth-Science Reviews,
967 66, 89-141.

968 Möller P., Dulsky P., Morteani G., 2003. Partitioning of rare earth elements, yttrium, and some
969 major elements among source rocks, liquid and vapor of Larderello-Travale Geothermal Field,
970 Tuscany (Central Italy). Geochimica et Cosmochimica Acta, 67 (2), 171–183.
971 Nappi G., A. Renzulli, P. Santi and P.Y. Gillot, 1995. Geological evolution and geochronology of
972 the Vulsini Volcano District (Central Italy). Bollettino della Società Geologica Italiana, 114,
973 599-613.
974 Panichi C., Tongiorgi E., 1976. Carbon isotopic composition of CO2 from springs, fumaroles,
975 mofettes and travertines of central and southern Italy: a preliminary prospection method of
976 geothermal area. Proc. 2nd UN Symposium on the Development and Use of Geothermal
977 Energy. San Francisco, U.S.A, 815–825.
978 Pascucci V., Costantini A., Martini P.I., Dringoli R., 2006. Tectono-sedimentary analysis of a
979 complex, extensional, Neogene basin formed on thrust-faulted, Northern Apennines
980 hinterland: Radicofani Basin, Italy. Sedimentary Geology, 183, 71–97.
981 Passchier C.W., Trouw R.A.J., 1996. Microtectonics. Springer Verlag, Berlin.
982 Patacca E., Sartori R., Scandone P., 1990. Tyrrhenian basin and Apenninic arcs: kinematic relation
983 since late Tortonian times. Memorie della Società Geologica Italiana, 45, 425-451.
984 Pauselli C., Barchi M.R., Federico C., Magnani B., Minelli G., 2006. The crustal structure of the
985 Northern Apennines (central Italy): an insight by the CROP03 seismic line. American Journal
986 of Science, 306, 428-450.
987 Peccerillo A., 2003. Plio-Quaternary magmatism in Italy. Episodes, 26, 222-226.
988 Pentecost A., 1995. The Quaternary travertine deposits of Europe and Asia Minor. Quaternary
989 Science Reviews, 14, 1005–1028.
990 Pentecost A., 2005. Travertine. Springer-Verlag, Berlin Heidelberg, 445 pp.
991 Pin C., Zalduegui J.F.S., 1997. Sequential separation of light rare-earth elements, thorium and
992 uranium by miniaturized extraction chromatography: Application to isotopic analyses of
993 silicate rocks. Analytica Chimica Acta, 339, 79-89.

994 Priewisch A., Crossey L.J., Karlstrom K.E., Polyak V.J., Asmerom Y., Nereson A., Ricketts J.W.,
995 2014. U-series geochronology of large-volume Quaternary travertine deposits of the
996 southeastern Colorado Plateau: Evaluating episodicity and tectonic and paleohydrologic
997 controls. Geosphere, 10, 401-423.
998 Rimondi V., Costagliola P., Ruggieri G., Benvenuti M., Boschi C., Brogi A., Capezzuoli E., Morelli
999 G., Gasparon M., Liotta D., 2015. Investigating fossil hydrothermal systems by means of fluid
1000 inclusions and stable isotopes in banded travertine: an example from Castelnuovo dell'Abate
1001 (southern Tuscany, Italy). International Journal of Earth Sciences, 1-21.
1002 Rezende M.F., Pope M.C., 2015. Importance of depositional texture in pore characterization of
1003 subsalt microbialite carbonates, offshore Brazil. Geological Society, London, Special
1004 Publication, 418, doi:10.1144/SP418.2.
1005 Ricketts J.W., Karlstrom K.E., Priewisch A., Crossey L.J., Polyak V.J., Asmerom Y., 2014.
1006 Quaternary extension in the Rio Grande rift at elevated strain rates recorded in travertine
1007 deposits, central New Mexico. Lithosphere, 6, 3–16.
1008 Rihs S., Condomines M., Poidevin J.L., 2000. Long-term behaviour of continental hydrothermal
1009 systems: U-series study of hydrothermal carbonates from the French Massif Central (Allier
1010 Valley). Geochimica et Cosmochimica Acta, 64 (18), 3189-3199.
1011 Roedder E. 1967. Metastable Superheated Ice in Liquid-Water Inclusions under High Negative
1012 Pressure. Science, 155, No. 3768, 1413-1417.
1013 Rogie J. D., Kerrick D. M., Chiodini G., Frondini F., 2000. Measurements of non-volcanic CO_2
1014 emission from some vents in central Italy, Journal of Geophysical Research, 105, 8435–8445.
1015 Ronchi P., Cruciani F., 2015. Continental carbonates as a hydrocarbon reservoir, an analog case
1016 study from the travertine of Saturnia, Italy. AAPG Bulletin, 99, 711–734.
1017 Rossetti F., Balsamo F., Villa I.M., Bouybaouenne M., Faccenna C., Funiciello R., 2008. Pliocene–
1018 Pleistocene HT–LP metamorphism during multiple granitic intrusions in the southern branch

of the Larderello geothermal field (southern Tuscany, Italy). Journal of the Geological Society, London, 165, 247-262.

Rossetti F., Aldega L., Tecce F., Balsamo F., Billi A., Brilli M., 2011. Fluid flow within the damage zone of the Boccheggiano extensional fault (Larderello–Travale geothermal field, central Italy): structures, alteration and implications for hydrothermal mineralization in extensional settings. Geological Magazine, 148 (4), 558–578.

Serri G., Innocenti F., Manetti P., 1993. Geochemical and petrological evidence of the subduction of delaminated Adriatic continental lithosphere in the genesis of the Neogene-Quaternary magmatism in central Italy. Tectonophysics, 223, 117– 147.

Serri G., 1997. Neogene–Quaternary magmatic activity and its geodynamic implications in the Central Mediterranean region. Annals of Geophysics, 40, 681–703.

Sharma M. and Wasserburg G.J., 1996. The neodymium isotopic compositions and rare earth patterns in highly depleted ultramafic rocks. Geochimica et Cosmochimica Acta, 60, 4537–4550.

Shen C.-C., Cheng H., Edwards R.L., Moran S.B., Edmonds H.N., Hoff J.A., Thomas R.B., 2003. Measurement of attogram quantities of ^{231}Pa in dissolved and particulate fractions of seawater by isotope dilution thermal ionization mass spectroscopy. Analytical Chemistry, 75, 1075-1079.

Shen C.-C., Wu C.-C., Cheng H., Edwards R.L., Hsieh Y.-T., Gallet S., Chang C.-C., Li T.-Y., Lam D.D., Kano A., Hori M., Spötl C., 2012. High-precision and high resolution carbonate ^{230}Th dating by MC-ICP-MS with SEM protocols. Geochimica et Cosmochimica Acta, 99, 71–86.

Shipton Z.K., Evans J.P., Kirchner D., Kolesar P.T., Williams A.P., Heath J., 2004. Analysis of CO_2 leakage through "low-permeability" faults from natural reservoirs in the Colorado Plateau, southern Utah. Geological Society, London, Special Publications, 233, 43-58.

1043 Shipton Z.K., Evans J.P., Dockrill B., Heath J., Williams A., Kirchner D., Kolesar P.T., 2005.
1044 Natural leaking CO_2-charged systems as analogs for failed geologic storage reservoirs. Carbon
1045 dioxide capture for storage in deep geological formations, 2, 699-712.
1046 Sibson R. H., 2004. Controls on maximum fluid overpressure defining conditions for mesozonal
1047 mineralization. Journal of Structural Geology, 26, 1127–1136
1048 Słowakiewicz M., 2003. Fluid inclusion data from the Upper Triassic hot-spring travertines in
1049 southern Poland. Journal of Geochemical Exploration, 78–79, 123-126.
1050 Soligo M., Tuccimei P., Barberi R., Delitala M.C., Miccadei E., Taddeucci A., 2002. U/Th dating of
1051 freshwater travertine from Middle Velino Valley (Central Italy): paleoclimatic and geological
1052 implications. Palaeogeography, Palaeoclimatology, Palaeoecology, 184, 147-161.
1053 Sturchio, N.C., Pierce, K.L., Murrell, M.T., Sorey, M.L., 1994. Uranium-series ages of travertines
1054 and timing of the last glaciation in the northern Yellowstone area, Wyoming– Montana.
1055 Quaternary Research, 41, 265–277.
1056 Toker E., Kayseri-Özer M. S., Özkul M., Kele S., 2015. Depositional system and palaeoclimatic
1057 interpretations of Middle to Late Pleistocene travertines: Kocabaş, Denizli, south-west Turkey.
1058 Sedimentology, 62, 1360-1383.
1059 Turi B., 1986: Stable isotope geochemistry of travertines: chapter 5. In: Fritz, P., Fontes, J.C (Eds.).
1060 The Terrestrial Environment, B, Handbook of Environmental Isotope Geochemistry, vol. 2.
1061 Elsevier, Amsterdam, pp 207–238.
1062 Tzedakis P.C., Andrieu V., de Beaulieu J.-L., Birks H.J.B., Crowhurst S., Follieri M., Hooghiemstra
1063 H., Magri D., Reille M., Sadori L., Shackleton N.J., Wijmstra T.A., 2001. Establishing a
1064 terrestrial chronological framework as a basis for biostratigraphical comparisons. Quaternary
1065 Science Reviews, 20, 1583-1592.
1066 Uysal I.T., Feng Y., Zhao J.X., Altunel E., Weatherley D., Karabacak V., Cengiz O., Golding S.D.,
1067 Lawrence M.G., Collerson K.D., 2007. U-series dating and geochemical tracing of late

Quaternary travertine in co-seismic fissures: Earth and Planetary Science Letters, 257 (3–4), 450–462.

Uysal I.T., Feng Y., Zhao J.X., Isik V., Nuriel P., Golding S.D., 2009. Hydrotermal CO_2 degassing in seismically active zones during the late Quaternary. Chemical Geology, 265, 442–454.

Webb G.E., Kamber B.S. , 2000 Rare earth elements in Holocene reefal microbialites: a shallow seawater proxy. Geochimica et Cosmochimica Acta, 64, 1557–1565.

Wedepohl K., 1995. The composition of the continental crust. Geochimica et Cosmochimica Acta, 59, 1217–1239.

Yilmaz T.I., Prosser G., Liotta D., Kruhl J.H., Gilg H.A., 2014. Repeated hydrothermal quartz crystallization and cataclasis in the Bavarian Pfahl shear zone (Germany). Journal of Structural Geology, 68, 158-174

Zanchi A., Tozzi M., 1987. Evoluzione paleogeografica e strutturale recente del bacino del fiume Albegna (Toscana meridionale). Geologica Romana 26, 305–325.

Appendix: geochemical methods

U/Th dating

As reported in Tables 2 and S1, we performed U/Th dating analyses using two different methods, namely (1) through α spectrometry performed at the Laboratorio di Geochimica Ambientale e Isotopica of Roma Tre University (Italy), or (2) through a Thermo Electron Neptune multi-collector inductively coupled mass spectrometer (MC-ICP-MS) (Shen et al., 2012) hosted at the High-Precision Mass Spectrometry and Environment Change Laboratory (HISPEC) of the National Taiwan University, Taipei (Taiwan ROC).

For MC-ICP-MS dating, we covered about 0.05 g of each sample with H_2O and dissolved it gradually with double distilled 14 N HNO_3. After dissolution, we added a ^{229}Th-^{233}U-^{236}U spike (Shen et al., 2003) to the sample, followed by 10-20 drops of $HClO_4$ to clear the organic matter. We then followed the chemical procedure described in Shen et al. (2003) for the separation of Uranium and Thorium. We calculated the age correction using an estimated atomic $^{230}Th/^{232}Th$ ratio of 4 ± 2 ppm. These latter values are the ones typical for a material at secular equilibrium with the crustal $^{232}Th/^{238}U$ value of 3.8. We arbitrarily assumed a 50% error.

For α spectrometry dating, we dissolved about 60 g of each sample in 7 N HNO_3 and filtered the solution to separate the leachates from the insoluble residue. We heated the leachate at 200 °C after adding a few millilitres of hydrogen peroxide to clear the organic matter, and then spiked the solution with a ^{228}Th-^{232}U tracer. We extracted the isotopic complexes of U and Th following the procedure described in Edwards et al. (1988) and then analyzed the solution by an alpha-counted using high-resolution ion-implanted Ortec silicon-surface barrier detectors. Due to the presence of non-radiogenic ^{230}Th related to detrital ^{232}Th, ages obtained for samples with a $^{230}Th/^{232}Th$ activity ratio less than or equal to 80 required a proper correction, which we performed assuming that all the detrital Th had an average $^{230}Th/^{232}Th$ activity ratio of 0.85 ± 0.36 (Wedepohl, 1995), which is the crustal thorium mean composition. We then calculated the ages using ISOPLOT, a plotting and regression program for radiogenic-isotope data (Ludwig, 2003).

C- and O-isotope determination

The isotopic composition of carbonate was measured according to the method described in detail in Breitenbach and Bernasconi (2011). Briefly, approximately 100 µg of powder were filled in 12 ml Exetainers (Labco, High Wycombe, UK) and flushed with pure Helium. The samples were reacted with 3-5 drops of 100% phosphoric acid at 70°C with a ThermoFisher GasBench device connected to a ThermoFisher Delta V mass spectrometer. The average long term reproducibility of the measurements based on replicated standards was ±0.05‰ for $\delta^{13}C$ and ±0.06‰ for $\delta^{18}O$. The instrument is calibrated with the international standards NBS19 ($\delta^{13}C$= 1.95 and $\delta^{18}O$ = -2.2‰) and NBS18 ($\delta^{13}C$= -5.01 and $\delta^{18}O$ = -23.01‰). The isotope values are reported in the conventional delta notation with respect to VPDB (Vienna Pee Dee Belemnite).

Thermometry of mineralizing parental fluids from O-isotopes

We calculated the paleo-temperature of mineralizing parental fluids using the equation of Kele et al. (2015) specifically developed for travertine parental fluids and calibrated through clumped isotope thermometer. This empirical equation is expressed as:

$$1000\ln \alpha_{(calcite\text{-}water)} = (20 \pm 2)\ 1000/T - (36 \pm 7) \qquad \text{(Eq.3)}$$

Where (1) $\alpha_{(calcite\text{-}water)} = (\delta^{18}O_{calcite} + 1000) / (\delta^{18}O_{water} + 1000)$, (2) T is the temperature of the mineralizing $CaCO_3$-rich fluids expressed in K and (3) $\delta^{18}O_{calcite}$ and $\delta^{18}O_{water}$ are expressed in parts ‰ relative to V-SMOW. As benchmark ($\delta^{18}O_{water}$), we measured and used the present $\delta^{18}O$ isotopic value from the Saturnia spring hydrothermal waters (-6.4‰ V-SMOW), whose active source is located 9 km to the south of the Semproniano giant vein. We assume that the oxygen isotope composition of the palaeosprings was similar to those of the current springs.

Sr- and Nd-isotope and REE determination

We determined the Strontium (Sr) and Neodymium (Nd) isotope ratios as well as Strontium, rare Earth elements (REE) and Yttrium (Y) concentrations on fragments of handpicked travertine and vein samples. We crushed the chips of travertine in a stainless steel mortar and then we dissolved about 200 mg of each sample with ultrapure HNO_3 (3%). We splitted 100 ml of solution from each sample into two aliquots. We used one of the two aliquots for REE, Y, and Sr concentrations and the other aliquot for Sr and Nd isotopes. The aliquot for REE, Y and Sr concentration were analyzed via ICP-MS (Agilent mod. 7500ce) equipped with collision cell at the Chemical Laboratory of Istituto di Chimica Agraria ed Ambientale, Catholic University of Piacenza and Cremona (Italy). We evaporated the aliquot for isotope analysis, converted it into chloride form, and loaded it onto standard Bio-Rad AG50W-X12 cation exchange resin to separate Sr from matrix. The very low REE and Y (REY) contents in travertine required the procedure of Sharma and Wasserburg (1996): we added ultrapure NH_3 to the solution diluted with MilliΩ water up to ionic strength of about 1.0 to shift pH to 9.0 for precipitating REY with Fe oxide-hydroxides. We then mixed both the precipitate and the supernatant with a vortex overnight and separated from each other by filtration. We dissolved the oxide-hydroxides with 4M HCl and separated them from the matrix via ion-exchange chromatography. We separated Nd from the other REE with Ln. Spec resin (Triskem-international) following the procedure of Pin and Zalduegui (1997).

We carried out the isotopic analyses at Istituto di Geologia Ambientale e Geoingegneria – Consiglio nazionale delle Ricerche (IGAG-CNR) laboratory c.o. Dipartimento di Scienze della Terra, Sapienza University of Rome (Italy) using a FINNIGAN MAT 262RPQ multicollector mass spectrometer. We loaded all samples on a Re double filament as nitrate and analyzed them in static mode. We normalized Sr analyses to $^{86}Sr/^{88}Sr = 0.1194$. We fixed Sr analytical blank at 1ng. Internal precision ("within-run" precision) of a single analytical result is given as two standard error of the mean (2se) and is obtained as a mean of more than 200 ratios collected on each sample with a stable bean of 2.0 V.

Repeated analyses of NIST-987 during the period of the analyses gave a mean value of $^{87}Sr/^{86}Sr = 0.710235 \pm 9$ (n = 20) and La Jolla $^{143}Nd/^{144}Nd = 0.511851 \pm 10$ (n=20), $^{146}Nd/^{144}Nd$ normalized to 0.7219. Total procedural blanks were below 2 ng of Sr and 1 ng of Nd for all the samples. The measured $^{143}Nd/^{144}Nd$ ratios are presented as fractional deviation in parts in 10^4 (ε-units) from $^{143}Nd/^{144}Nd$ in a Chondritic Uniform Reservoir (CHUR) as measured today:

$$\varepsilon_{Nd\,(0)} = [(^{143}Nd/^{144}Nd)_{sample} / (^{143}Nd/^{144}Nd)_{CHUR} - 1] \times 10^4 \qquad \text{(Eq.4)}$$

where $(^{143}Nd/^{144}Nd)_{sample}$ is the ratio measured in the sample today and $(^{143}Nd/^{144}Nd)_{CHUR}$ is the ratio in the reference reservoir today, i.e. 0.511847 (DePaolo and Wasserburg, 1976).

Fluid inclusion analysis

We performed microthermometric measurements at Istituto di Geologia Ambientale e Geoingegneria – Consiglio nazionale delle Ricerche (IGAG-CNR) Fluid Inclusion Laboratory c/o Dipartimento di Scienze della Terra, Sapienza University of Rome (Italy), using a freezing-heating stage Linkam THMSG600 (from -196 to +600 °C). The stage is adapted to a Nikon Optiphot-Pol transmitted-light microscope equipped with long-working distance objectives (5X, 10X, 20X, and 40X) and a video camera. We performed the analysis of fluid inclusions on a 150 μm thick double-polished slice of calcite vein (Fig. 9). Due to the physical properties of calcite minerals, we took particular care in maintaining as low as possible the temperature during grinding, polishing, and, in general, during all the sample preparation (Goldtsein and Reynolds, 1994; Bodnar, 2003). A low-temperature sample preparation is fundamental to avoid phenomena of stretching and decrepitation of the inclusions, which may affect the microthermometric measurements. In those fluid inclusions where decrepitation and stretching phenomena due to the volume expansion during ice formation (Bodnar, 2003) were visible, we perform Tm_{ice} measurements separately from Th measurements. Salinity contents (expressed in wt% NaCl eq.) of fluid inclusions has been calculated through the Tm_{ice} values using the equation proposed by Bodnar and Vityk (1994). Data reproducibility is of ± 0.2 °C for cooling runs and of ± 1 °C for heating runs.

Figure Captions

Figure 1. (a) Schematic map of Italy showing the Apennines fold-thrust belt and the area affected by crustal extension at the rear (west) of the belt. This latter area includes Tuscany, where the study area (Semproniano, upper Albegna basin, southern Tuscany) is located. **(b)** Geological map of the southern Tuscany and northern Latium regions showing the main geothermal fields and travertine deposits (including fissure ridges).

Figure 2. (a) Structural geological map of the study area (Semproniano area in the upper Albegna basin) and **(b)** related geological cross-sections. The map is based on and partly redrawn from the geological map at the 1:10,000 scale available online at www.regione.toscana.it/-/geologia.

Figure 3. (a) Northward panoramic view of the study area with localization of the studied travertine deposits that are differentiated by morphology. **(b)** Northward panoramic view of the Semproniano ridge (i.e., Semproniano giant vein). Tracks of geological cross-sections (Figs. 2b and 6) are also shown.

Figure 4. (a) Southward panoramic view of Poggio i Piani and Poggio Semproniano travertine plateaus. The Poggio i Piani plateau lies on top of the Scaglia Toscana Fmt. (belonging to the non-metamorphic succession of the Tuscan Domain) whereas the Poggio Semproniano plateau lies on top of Plio-Quaternary marine deposits. **(b)** Southern margin of the Poggio Semproniano travertine plateau. **(c)** Sub-horizontal travertine beds forming the Poggio I Piani plateau. **(d)** Detail of a laminated bedded travertine from Poggio I Piani plateau. **(e)** Close-up view of the bedded travertine occurring at Poggio i Piani.

Figure 5. (a) Panoramic view of the Semproniano giant vein and travertine plateau (Poggio Semproniano). **(b)** Attitude of the sparry bands (banded travertine) forming the Semproniano giant vein (NE flank). This exposure is located below the fortress of the Aldobrandeschi family (X century) in the Semproniano village. **(c)** The Semproniano giant vein (banded travertine) is mainly oriented NW-SE and characterized by high dip values (see the stereoplot: Schmidt net, lower hemisphere, showing poles to travertine subvertical bands forming the giant vein). **(d)** Detail from the Semproniano giant vein (banded travertine) with indication of the vein growth. **(e)** The central part of the Semproniano giant vein shows a V-like shape and is characterized by a rhythmic sequence of crystallized subvertical bands of sparry carbonate. Sample SP12, used for fluid inclusion analysis, was collected here. **(f)** Spatial relationships between banded and bedded travertine along the flank of the Semproniano giant vein. **(g)** Sub-horizontal, bedded travertine exposed on the south-western flank of the Semproniano giant vein. **(h)** Sub-horizontal, bedded travertine cut through by bedded parallel travertine veins (Semproniano village). **(i)** Bedded travertine fabric characterized by laminations, shrubs, and karst-dissolution cavities (Semproniano village). **(j)** and **(k)** Travertine veins cutting through carbonate rocks (Tuscan Domain) along the SW flank of the Semproniano giant vein. Cross-cutting relationships between travertine veins show multiple phases of veining.

Figure 6. (a) Panoramic view of the Semproniano-Poggio Semproniano area where the traces of the main fault systems (*ca*. E-W- and N-S-striking) are indicated. The stereoplots (Schmidt net, lower hemisphere) show attitude of the measured structural features. **(b)** The E-W-striking fault system affecting the bedded travertine at Poggio Semproniano is characterized by meter-thick damage zone and narrowly-spaced fault surfaces. **(c)** Fault surfaces are equipped with oblique- to strike-slip striations (pitch is generally higher than 160° or lesser than 20°; see the stereoplot). Right-lateral strike-slip kinematics has been documented for this fault system. **(d)** The N-S-striking fault across the banded travertine of the Semproniano village is defined by a half-meter-thick damage zone and

secondary fracture network. Extensional kinematics (associated to a left-lateral movement) has been documented for this fault system.

Figure 7. (a) Photomosaic (above) and related line drawing (below) of the Semproniano giant vein as it is exposed in the upper part of the Semproniano village. **(b)** Conceptual cross-sectional sketch of the Semproniano giant vein that is made of an uninterrupted swarm of sparry bands (banded travertine). Sample location and related radiometric ages are shown both in (a) and in (b).

Figure 8. (a) Panoramic view (Google Earth image) with localization of the studied travertine deposits (same as Fig. 3a). **(b)** Combined plot of $\delta^{13}C$ (‰ V-PDB) and $\delta^{18}O$ (‰ V-PDB) isotope values derived from samples of bedded and banded travertines and calcite veins (Table 3). **(c)** Plot of calculated temperatures for the parental fluids of the studied travertines and $CaCO_3$ precipitates (Table 3). **(d)** Combined plot of parental fluid temperatures and U/Th ages determined on the same samples.

Figure 9. Post Archean Australian shale (PAAS) – normalized REY pattern (rare Earth elements + Yttrium) for: the Semproniano giant vein (banded travertine); the bedded travertine flanking the giant vein; bedded travertine and calcite vein from Poggio Semproniano; and banded travertine from I Vignacci. For comparison, REE data from the Tuscan Nappe limestone are also shown (data from Möller et al., 2003).

Figure 10. (a) Close up photograph of banded travertine from the central part of the Semproniano giant vein. The sample studied for fluid inclusions comes exactly from the spot shown in the photograph. **(b)**, **(c)**, and **(d)** Microphotographs (transmitted light, parallel nicols) of liquid-rich fluid inclusions hosted in the banded travertine shown in the previous close-up photograph. L and V are for liquid and vapor phases, respectively, within the studied inclusions. **(e)** and **(f)** Results of

microthermometry on fluid inclusions hosted in elongate calcite crystals. Th is the temperature (°C) of homogenization whereas Tm_{ice} (°C) is the temperature of last melting of ice.

Figure 11. Comparison between U/Th ages of bedded travertine, banded travertine, and calcite veins from the study area and major paleoclimate indicators represented by the deep sea oxygen isotope trend (Zachos et al., 2001) and by the pollen dataset from Valle di Castiglione (Tzedakis et al., 2001). Global glacial/interglacial periods are redrawn and modified after Priewish et al (2014).

Figure 12. (a) Schematic 3D-block diagram interpreting the hydrothermal settingin the Mt. Amiata-Semproniano area. Active faulting and related fracturation have primary role in controlling meteoric percolation within the carbonate reservoir at depth, and the uprise of hydrothermal fluids. **(b)** Two-step scenario illustrating the mode of travertine deposition (by veining at Semproniano fissure ridge and by dominant progradation at the Poggio Semproniano plateau) supplied by hydrothermal fluid discharge at the fault/fracture tips. The fault architecture is indicative.

Table Captions

Table 1. Samples, sampling sites, and laboratory analyses.

Table 2. U/Th Age of travertines sampled in the study area. See Table S1 for a complete list of data. Samples indicated with * were analyzed through MC-ICP-MS at the HISPEC lab of the National Taiwan University (errors quoted as 2σ), whereas samples indicated with ** were analyzed through α spectrometry at the Laboratorio di Geochimica Ambientale e Isotopica of Roma Tre University, Italy (errors quoted as 1σ).

Table 3. Stable oxygen and carbon isotope composition, and paleotemperature of banded travertine, bedded travertine, and calcite veins from the study area. Isotope compositions are expressed in ‰ against Vienna Pee Dee Belemnite standard (V-PDB) and in ‰ against Vienna Standard Mean Ocean Water (V-SMOW). Temperature of parental fluids derive from $\delta^{18}O$ through the equation of Kele et al. (2015). $\delta^{13}C_{Co2}$* have been calculated using the empirical equation of Panichi and Tongiorgi. (1976). $\delta^{13}C_{Co2}$** have been calculated using the theoretical equation of Bottinga (1968).

Table 4. Strontium, Strontium isotopes and Neodymium isotopes measured on selected samples from travertines of the study area.

Table S1. Uranium isotopic composition and ^{230}Th ages for travertines of Semproniano Village, Poggio Semproniano, Poggio I Piani and I Vignacci. Samples marked with * were analysed through MC-ICP-MS. Age correction were calculated using an estimated atomic $^{230}Th/^{232}Th$ ratio of 4 ± 2 ppm. Those are the values for a material at secular equilibrium with the crustal $^{232}Th/^{238}U$ value of 3.8. The errors are arbitrarily assumed to be 50%. Samples marked with ** were analysed through alpha spectrometry. The ($^{230}Th/^{234}U$) was corrected using the crustal thorium mean composition. 0.85 ± 0.36 (Wedephol. 1995), for samples with a $^{230}Th/^{232}Th$ activity ratio lower than 80.

Table S2. Concentration or rare earth elements and yttrium for travertine samples of the study area (in μg/kg).

Table 1
Click here to download Table: Semproniano_Table1_Berardi et al.docx

Table 1. Samples, sampling sites, and laboratory analyses.

Sample	Locality	Rock Type	$\delta^{13}C$ (‰ V-PDB)	$\delta^{18}O$ (‰ V-PDB)	$^{87}Sr/^{86}Sr$	$^{143}Nd/^{144}Nd$	REE	U/Th
SP1	Semproniano Village	Banded Travertine	X	X				X
SP5	Semproniano Village	Banded Travertine	X	X				
SP6	Semproniano Village	Banded Travertine	X	X				
SP7	Semproniano Village	Banded Travertine	X	X				
SP8	Semproniano Village	Banded Travertine	X	X				
SP11	Semproniano Village	Bedded Travertine	X	X	X			X
SP12*	Semproniano Village	Banded Travertine	X	X	X			X
SP12B	Semproniano Village	Banded Travertine	X	X				
SP15	Semproniano Village	Banded Travertine	X	X				X
SP16	Semproniano Village	Calcite Vein	X	X				X
SP17	Semproniano Village	Bedded Travertine			X			
SP14/03	Semproniano Village	Banded Travertine	X	X				
SP14/04	Semproniano Village	Banded Travertine	X	X				
SP14/05	Semproniano Village	Bedded Travertine	X	X				
SP14/06	Semproniano Village	Bedded Travertine	X	X	X	X	X	
SP14/08	Semproniano Village	Banded Travertine	X	X				
SP14/09	Semproniano Village	Banded Travertine	X	X				
SP14/10	Semproniano Village	Banded Travertine	X	X				
SP14/11	Semproniano Village	Banded Travertine	X	X				
SP14/11B	Semproniano Village	Banded Travertine	X	X				
SP14/12	Semproniano Village	Banded Travertine	X	X				
SP14/13	Semproniano Village	Banded Travertine	X	X				
SP14/14	Semproniano Village	Banded Travertine	X	X				
SP14/15	Semproniano Village	Banded Travertine	X	X				X
SP14/16	Semproniano Village	Banded Travertine	X	X				
SP14/17	Semproniano Village	Banded Travertine	X	X				
SP14/18	Semproniano Village	Banded Travertine	X	X	X		X	X
SP14/19	Semproniano Village	Banded Travertine	X	X				
SP14/20	Semproniano Village	Banded Travertine	X	X				X
SP14/21	Semproniano Village	Banded Travertine	X	X				
SP14/22	Semproniano Village	Banded Travertine	X	X				
SP14/23	Semproniano Village	Banded Travertine	X	X				X
SP14/24	Semproniano Village	Banded Travertine	X	X				
SP14/25	Semproniano Village	Banded Travertine	X	X				X
SP14/26	Semproniano Village	Banded Travertine	X	X				
SP14/27	Semproniano Village	Banded Travertine	X	X				
SP14/28	Semproniano Village	Banded Travertine	X	X	X			X
SP14/29	Semproniano Village	Banded Travertine	X	X				
SP14/30	Semproniano Village	Banded Travertine	X	X				X
SP14/31	Semproniano Village	Banded Travertine	X	X				
SP14/32	Semproniano Village	Banded Travertine	X	X				X
SP14/33	Semproniano Village	Banded Travertine	X	X				
SP14/34	Semproniano Village	Banded Travertine	X	X				X
VI1	I Vignacci	Banded Travertine	X	X	X	X	X	X
SP3	Poggio Sempronian o	Calcite Vein	X	X	X	X	X	X
SP9	Poggio Sempronian o	Bedded Travertine	X	X	X			
SP10	Poggio Sempronian o	Calcite Vein	X	X	X			X
PS1	Poggio Sempronian o	Bedded Travertine	X	X				
PS2	Poggio Sempronian o	Bedded Travertine	X	X				
PS3	Poggio Sempronian o	Bedded Travertine	X	X				
PO1	Poggio Sempronian o	Bedded Travertine	X	X	X		X	
PO2	Poggio Sempronian o	Bedded Travertine	X	X	X			X
PP1	Poggio i Piani	Bedded Travertine	X	X				X

* In addition to the reported analyses, geothermometric determinations through fluid inclusion and clumped isotope analyses were done on this sample (SP12).

Table 2

Click here to download Table: Semproniano_Table2_Berardi et al.docx

Table 2. U/Th Age of travertines sampled in the study area. See Table S1 for a complete list of data. Samples indicated with * were analyzed through MC-ICP-MS at the HISPEC lab of the National Taiwan University (errors quoted as 2σ), whereas samples indicated with ** were analyzed through α spectrometry at the Laboratorio di Geochimica Ambientale e Isotopica of Roma Tre University, Italy (errors quoted as 1σ).

Sample	Location	Rock type	Age corrected (ka)
SP15*	Semproniano Village	banded travertine	**347 ± 22**
SP14/15*	Semproniano Village	banded travertine	**>800**
SP14/18*	Semproniano Village	banded travertine	**86 ± 1**
SP14/20*	Semproniano Village	banded travertine	**231 ± 9**
SP14/23*	Semproniano Village	banded travertine	**314 ± 11**
SP14/25*	Semproniano Village	banded travertine	**419 ± 39**
SP14/28*	Semproniano Village	banded travertine	**613 ± 200**
SP14/30*	Semproniano Village	banded travertine	**105 ± 1**
SP14/32*	Semproniano Village	banded travertine	***646***
SP14/34*	Semproniano Village	banded travertine	**495 ± 99**
SP1**	Semproniano Village	banded travertine	**>350**
SP12**	Semproniano Village	banded travertine	**128 ± 19**
SP16**	Semproniano Village	calcite vein	**104 ± 16**
SP11**	Semproniano Village	bedded travertine	**214 +50/-37**
SP3**	Poggio Semproniano	calcite vein	**43 ± 8**
SP10**	Poggio Semproniano	calcite vein	**39 ± 4**
PO2**	Poggio Semproniano	bedded travertine	**171 ± 19**
PP1**	Poggio i Piani	bedded travertine	**198 ± 18**
VI1**	Vignacci	banded travertine	**>350**

Table 3

Click here to download Table: Semproniano_Table3_Berardi et al.docx

Table 3. Stable oxygen and carbon isotope composition, and paleotemperature of banded travertine, bedded travertine, and calcite veins from the study area. Isotope compositions are expressed in ‰ against Vienna Pee Dee Belemnite standard (V-PDB) and in ‰ against Vienna Standard Mean Ocean Water (V-SMOW). Temperature of parental fluids derive from $\delta^{18}O$ through the equation of Kele et al. (2015). $\delta^{13}C_{Co2}$* have been calculated using the empirical equation of Panichi and Tongiorgi. (1976). $\delta^{13}C_{Co2}$** have been calculated using the theoretical equation of Bottinga (1968).

Sample	Locality	Rock Type	$\delta^{13}C$ (‰ V-PDB)	$\delta^{18}O$ (‰ V-PDB)	$\delta^{18}O$ (‰ V-SMOW)	$T_{calculated}$ (°C)	$\delta^{13}C_{Co2}$* (‰ V-PDB)	$\delta^{13}C_{Co2}$** (‰ V-PDB)
SP1	Semproniano Village	Banded Travertine	9.5	-12.7	17.8	60 ± 6	0.9	3.2
SP5	Semproniano Village	Banded Travertine	8.9	-10.8	19.8	49 ± 4	0.2	1.5
SP6	Semproniano Village	Banded Travertine	10.0	-12.2	18.3	57 ± 5	1.4	3.3
SP7	Semproniano Village	Banded Travertine	10.5	-11.6	19.0	53 ± 5	2.1	3.5
SP8	Semproniano Village	Banded Travertine	9.7	-12.3	18.2	58 ± 5	1.2	3.1
SP11	Semproniano Village	Bedded Travertine	9.9	-8.2	22.4	36 ± 2	1.4	1.1
SP12	Semproniano Village	Banded Travertine	4.9	-14.6	15.9	71 ± 7	-4.6	-0.5
SP12B	Semproniano Village	Banded Travertine	4.7	-13.5	17.0	64 ± 6	-4.9	-1.3
SP16	Semproniano Village	Calcite Vein	8.9	-12.0	18.6	56 ± 5	0.2	2.1
SP14/03	Semproniano Village	Banded Travertine	9.6	-12.3	18.2	58 ± 5	1.0	3.0
SP14/04	Semproniano Village	Banded Travertine	9.2	-12.7	17.8	60 ± 5	0.6	2.9
SP14/05	Semproniano Village	Bedded Travertine	5.8	-9.7	20.9	44 ± 3	-3.5	-2.2
SP14/06	Semproniano Village	Bedded Travertine	5.3	-9.8	20.9	44 ± 3	-4.2	-2.7
SP14/08	Semproniano Village	Banded Travertine	6.0	-9.8	20.8	44 ± 3	-3.3	-1.9
SP14/09	Semproniano Village	Banded Travertine	9.8	-11.1	19.5	51 ± 4	1.2	2.5
SP14/10	Semproniano Village	Banded Travertine	9.3	-10.9	19.7	50 ± 4	0.7	1.9
SP14/11	Semproniano Village	Banded Travertine	7.1	-11.1	19.5	51 ± 4	-2.1	-0.2
SP14/11B	Semproniano Village	Banded Travertine	6.0	-11.6	19.0	54 ± 5	-3.3	-1.0
SP14/12	Semproniano Village	Banded Travertine	9.2	-12.8	17.7	60 ±6	0.6	2.9
SP14/13	Semproniano Village	Banded Travertine	8.6	-12.3	18.3	57 ± 5	-0.2	2.0
SP14/14	Semproniano Village	Banded Travertine	7.7	-9.0	21.6	40 ± 3	-1.2	-0.7
SP14/15	Semproniano Village	Banded Travertine	8.0	-11.3	19.3	52 ± 5	-0.9	0.9
SP14/16	Semproniano Village	Banded Travertine	9.7	-10.1	20.5	46 ± 4	1.1	1.9
SP14/17	Semproniano Village	Banded Travertine	10.2	-10.7	19.9	49 ± 4	1.7	2.7
SP14/18	Semproniano Village	Banded Travertine	9.9	-10.6	20.0	48 ± 4	1.3	2.4
SP14/19	Semproniano Village	Banded Travertine	8.5	-10.7	19.9	49 ± 4	-0.3	1.1
SP14/20	Semproniano Village	Banded Travertine	8.2	-9.6	21.0	43 ± 3	-0.6	0.1
SP14/21	Semproniano Village	Banded Travertine	8.4	-12.1	18.5	56 ± 5	-0.4	1.7
SP14/22	Semproniano Village	Banded Travertine	10.1	-12.0	18.5	56 ± 5	1.6	3.3
SP14/23	Semproniano Village	Banded Travertine	7.0	-11.6	19.0	53 ± 5	-2.1	0.0

SP14/24	Semproniano Village	Banded Travertine	6.8	-11.3	19.2	52 ± 5	-2.3	-0.3
SP14/25	Semproniano Village	Banded Travertine	8.9	-9.9	20.7	45 ± 3	0.2	1.0
SP14/26	Semproniano Village	Banded Travertine	6.7	-11.4	19.2	52 ± 5	-2.5	-0.4
SP14/27	Semproniano Village	Banded Travertine	8.8	-10.7	19.9	49 ± 4	0.1	1.3
SP14/28	Semproniano Village	Banded Travertine	7.6	-10.0	20.6	45 ± 3	-1.4	-0.2
SP14/29	Semproniano Village	Banded Travertine	3.2	-8.8	21.8	39 ± 3	-6.7	-5.4
SP14/30	Semproniano Village	Banded Travertine	8.6	-11.2	19.4	51 ± 4	-0.2	1.4
SP14/31	Semproniano Village	Banded Travertine	6.5	-11.1	19.5	51 ± 4	-2.7	-0.8
SP14/32	Semproniano Village	Banded Travertine	9.0	-10.1	20.5	46 ± 4	0.3	1.2
SP14/33	Semproniano Village	Banded Travertine	6.3	-7.6	23.1	34 ± 2	-2.9	-2.9
SP14/34	Semproniano Village	Banded Travertine	6.5	-12.6	17.9	59 ± 5	-2.7	0.0
VI1	I Vignacci	Banded Travertine	3.7	-9.6	21.0	43 ± 3	-6.0	-4.4
SP3	Poggio Semproniano	Calcite Vein	7.1	-11.5	19.0	53 ± 5	-2.0	0.0
SP9	Poggio Semproniano	Bedded Travertine	6.8	-9.6	21.0	43 ± 3	-2.4	-1.3
SP10	Poggio Semproniano	Calcite Vein	8.4	-10.7	19.9	49 ± 4	-0.5	0.9
PS1	Poggio Semproniano	Bedded Travertine	6.9	-10.2	20.4	46 ± 4	-2.2	-0.8
PS2	Poggio Semproniano	Bedded Travertine	6.7	-8.1	22.6	36-± 2	-2.5	-2.3
PS3	Poggio Semproniano	Bedded Travertine	5.8	-10.1	20.5	46 ± 4	-3.6	-2.0
PO1	Poggio Semproniano	Bedded Travertine	5.6	-11.4	19.2	53 ± 5	-3.8	-1.5
PO2	Poggio Semproniano	Bedded Travertine	7.1	-9.8	20.8	44 ± 3	-2	-0.8
PP1	Poggio i Piani	Bedded Travertine	6.5	-11.6	19.0	53 ± 5	-2.7	-0.5

***(Panichi and Tongiorgi. 1976)**

**** (Bottinga, 1968)**

Table 4

Click here to download Table: Semproniano_Table4_Berardi et al.docx

Table 4. Strontium, Strontium isotopes and Neodymium isotopes measured on selected samples from travertines of the study area.

Sample	Locality	Rock Type	Sr (mg/kg)	$^{87}Sr/^{86}Sr \pm 2se^{*}$	$^{143}Nd/^{144}Nd \pm 2se^{*}$	$\varepsilon_{Nd\ i}$ **
SP12	Semproniano Village	Banded travertine	1189.46	0.708277 ± 11		
SP14/18	Semproniano Village	Banded travertine	1223.70	0.708395 ± 9		
SP14/28	Semproniano Village	Banded travertine	1125.91	0.708368 ± 10		
SP11	Semproniano Village	Bedded travertine	105.31	0.708491 ± 10		
SP14/06	Semproniano Village	Bedded travertine	652.35	0.708470 ± 5	0.512253 ± 18	-6.50
SP17	Semproniano Village	Bedded travertine	592.74	0.708437 ± 6		
SP9	Poggio Semproniano	Bedded travertine	734.74	0.708326 ± 7		
PO1	Poggio Semproniano	Bedded travertine	502.19	0.708334 ± 5		
PO2	Poggio Semproniano	Bedded travertine	787.25	0.708366 ± 7		
SP3	Poggio Semproniano	Calcite Vein	4763.20	0.708527 ± 7	0.512330 ± 39	-2.41
SP10	Poggio Semproniano	Calcite Vein	4154.77	0.708488 ± 9		
VI1	I Vignacci	Banded travertine	4956.30	0.708456 ± 6	0.512275 ± 20	-9.93

*Uncertainties are 2se mean, within-run precision and refer to the last digits

** ε_{Nd} has been calculated at 200Ma

Figure 1
Click here to download high resolution image

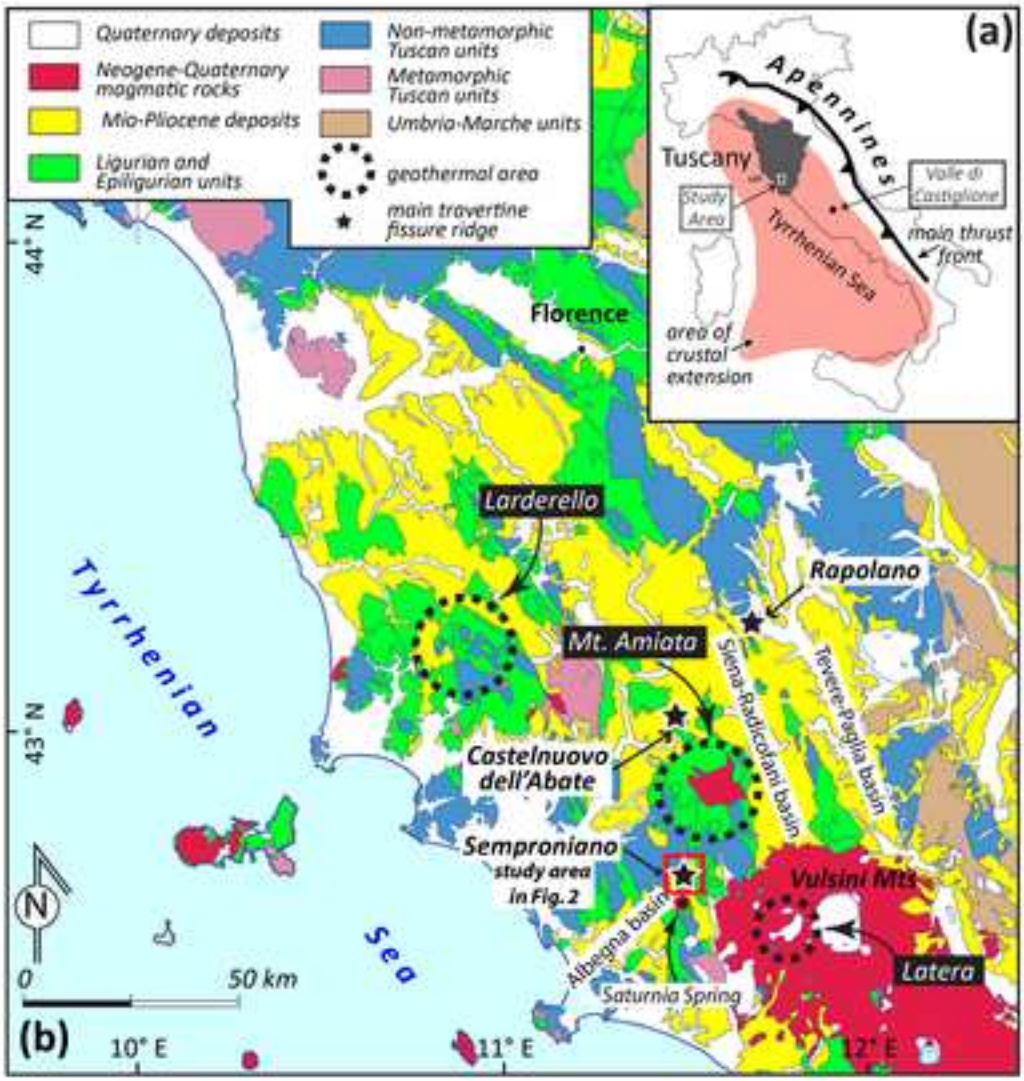

Figure 1. (a) Schematic map of Italy showing the Apennines fold-thrust belt and the area affected by crustal extension at the rear (west) of the belt. This latter area includes Tuscany, where the study area (Sempronian, upper Albegna basin, southern Tuscany) is located. **(b)** Geological map of the southern Tuscany and northern Latium regions showing the main geothermal fields and travertine deposits (including fissure ridges).

Figure 2
Click here to download high resolution image

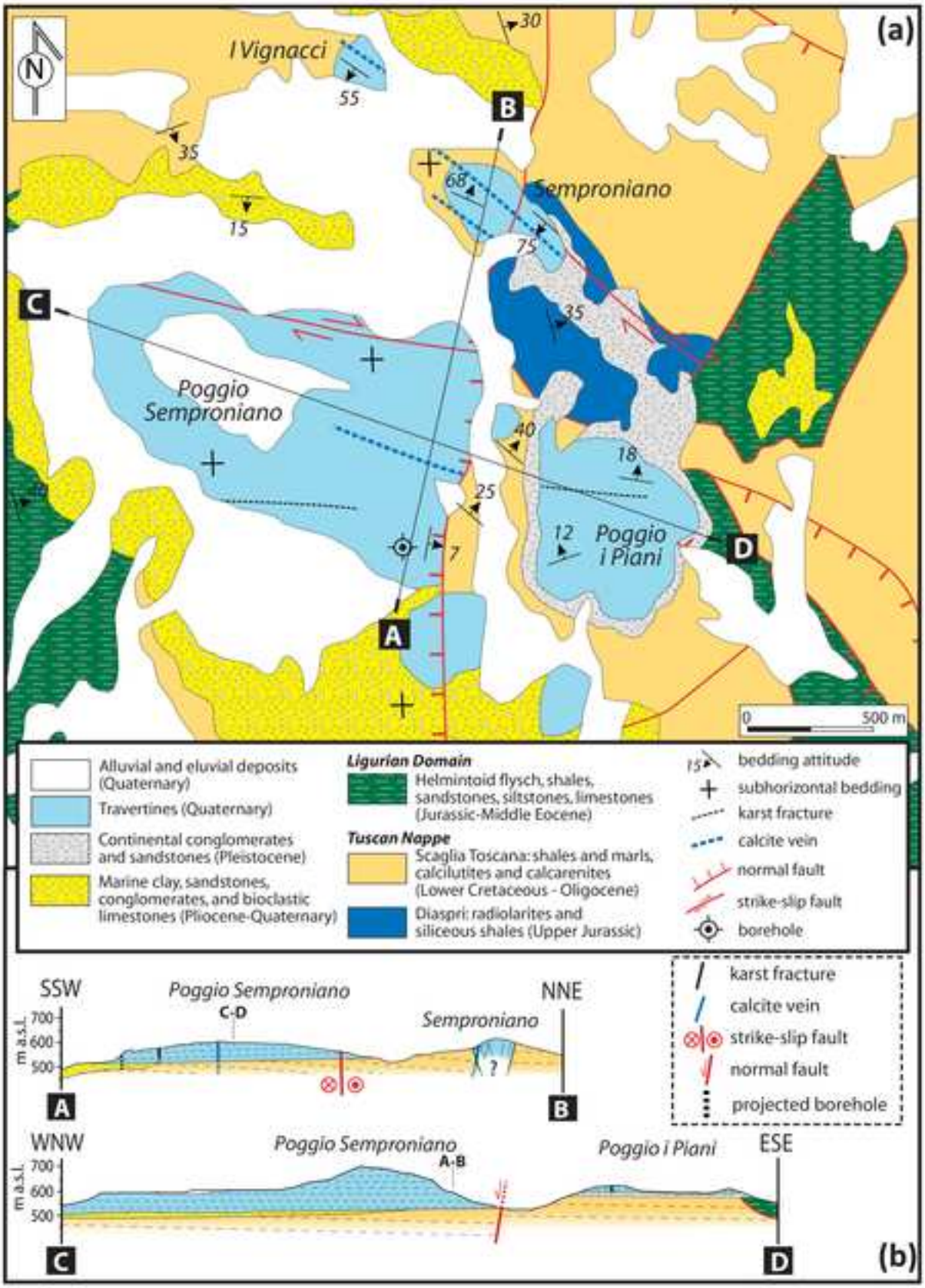

Figure 2. (a) Structural geological map of the study area (Semproniano area in the upper Albegna basin) and **(b)** related geological cross-sections. The map is based on and partly redrawn from the geological map at the 1:10,000 scale available online at www.regione.toscana.it/-/geologia.

Figure 3

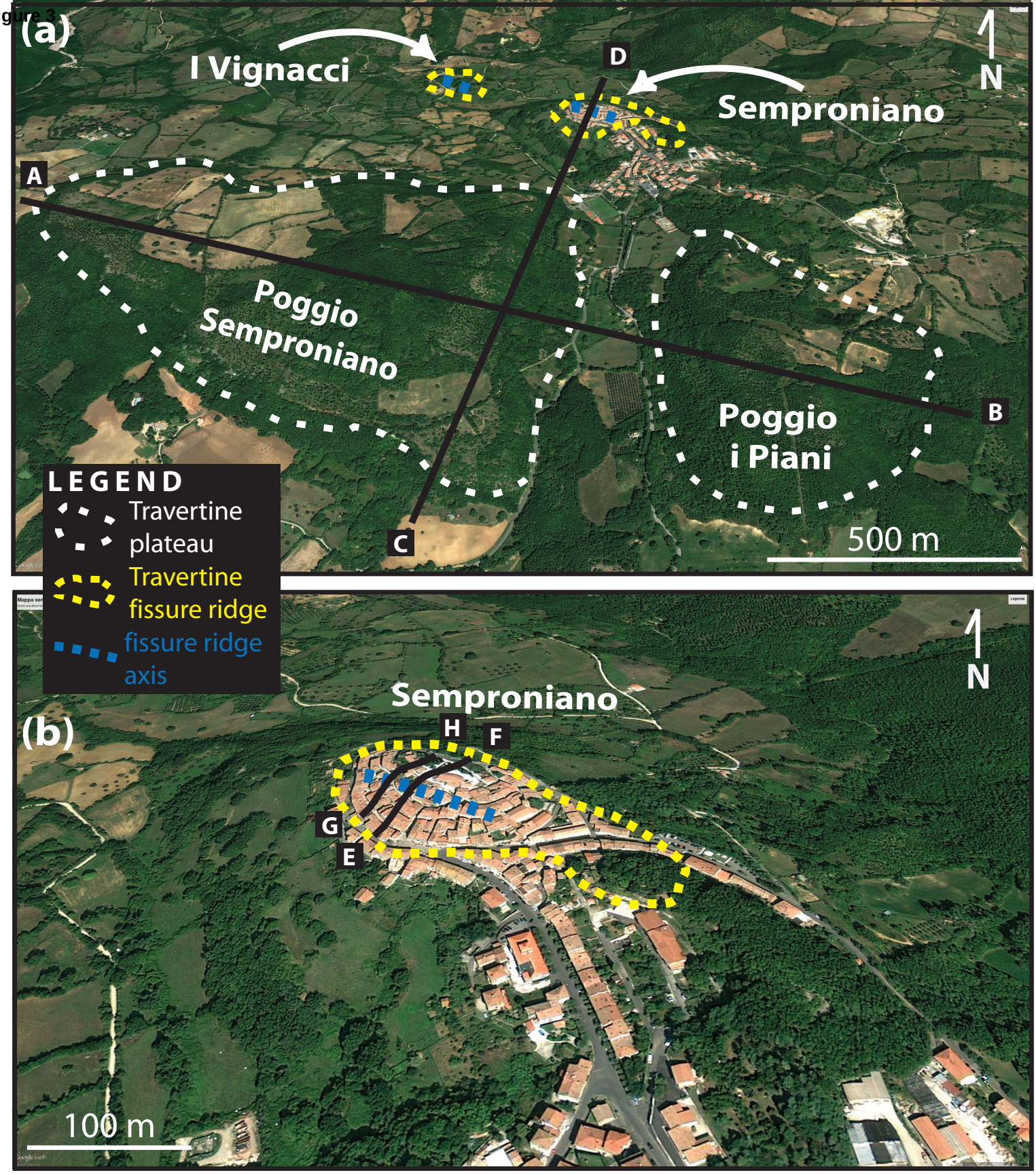

Figure 3. (a) Northward panoramic view of the study area with localization of the studied travertine deposits that are differentiated by morphology. **(b)** Northward panoramic view of the Sempronian ridge (i.e., Sempronian giant vein). Tracks of geological cross-sections (Figs. 2b and 6) are also shown.

Figure 4
Click here to download high resolution image

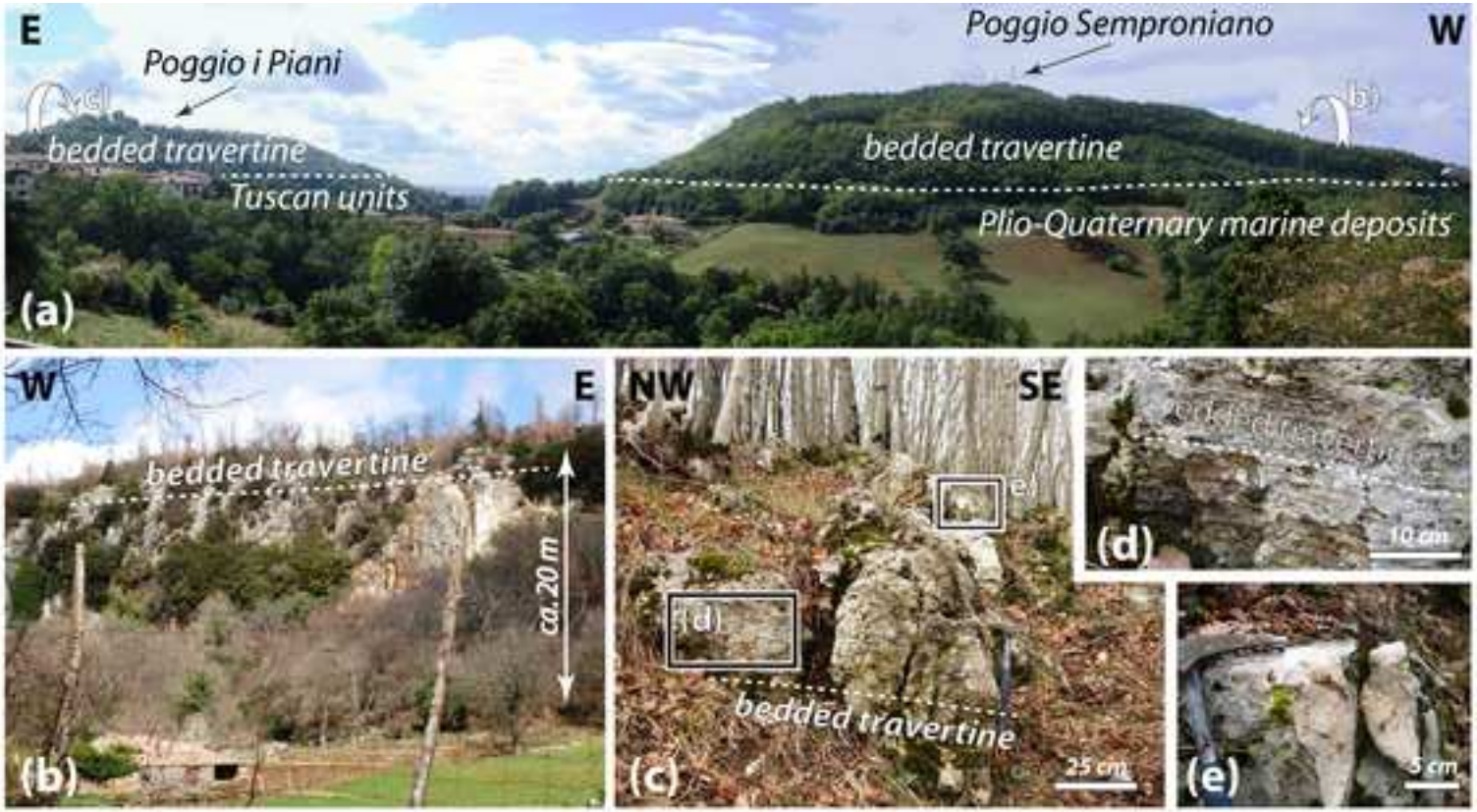

Figure 4. **(a)** Southward panoramic view of Poggio i Piani and Poggio Sempronian travertine plateaus. The Poggio i Piani plateau lies on top of the Scaglia Toscana Fmt. (belonging to the non-metamorphic succession of the Tuscan Domain) whereas the Poggio Sempronian plateau lies on top of Plio-Quaternary marine deposits. **(b)** Southern margin of the Poggio Sempronian travertine plateau. **(c)** Sub-horizontal travertine beds forming the Poggio I Piani plateau. **(d)** Detail of a laminated bedded travertine from Poggio I Piani plateau. **(e)** Close-up view of the bedded travertine occurring at Poggio i Piani.

Figure 5

Click here to download high resolution image

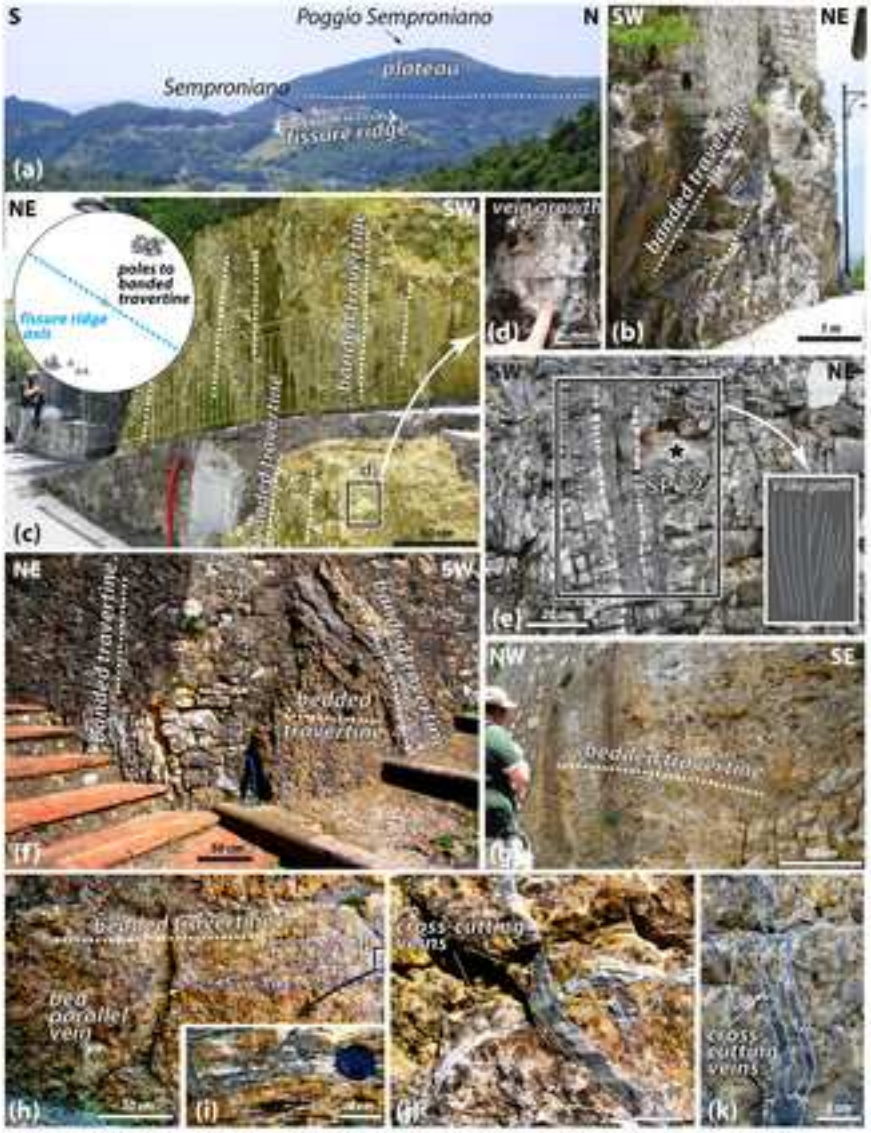

Figure 5. **(a)** Panoramic view of the Sempronian giant vein and travertine plateau (Poggio Sempronian). **(b)** Attitude of the sparry bands (banded travertine) forming the Sempronian giant vein (NE flank). This exposure is located below the fortress of the Aldobrandeschi family (X century) in the Sempronian village. **(c)** The Sempronian giant vein (banded travertine) is mainly oriented NW-SE and characterized by high dip values (see the stereoplot: Schmidt net, lower hemisphere, showing poles to travertine subvertical bands forming the giant vein). **(d)** Detail from the Sempronian giant vein (banded travertine) with indication of the vein growth. **(e)** The central part of the Sempronian giant vein shows a V-like shape and is characterized by a rhythmic sequence of crystallized subvertical bands of sparry carbonate. Sample SP12, used for fluid inclusion analysis, was collected here. **(f)** Spatial relationships between banded and bedded travertine along the flank of the Sempronian giant vein. **(g)** Sub-horizontal, bedded travertine exposed on the south-western flank of the Sempronian giant vein. **(h)** Sub-horizontal, bedded travertine cut through by bedded parallel travertine veins (Sempronian village). **(i)** Bedded travertine fabric characterized by laminations, shrubs, and karst-dissolution cavities (Sempronian village). **(j)** and **(k)** Travertine veins cutting through carbonate rocks (Tuscan Domain) along the SW flank of the Sempronian giant vein. Cross-cutting relationships between travertine veins show multiple phases of veining.

Figure 6
Click here to download high resolution image

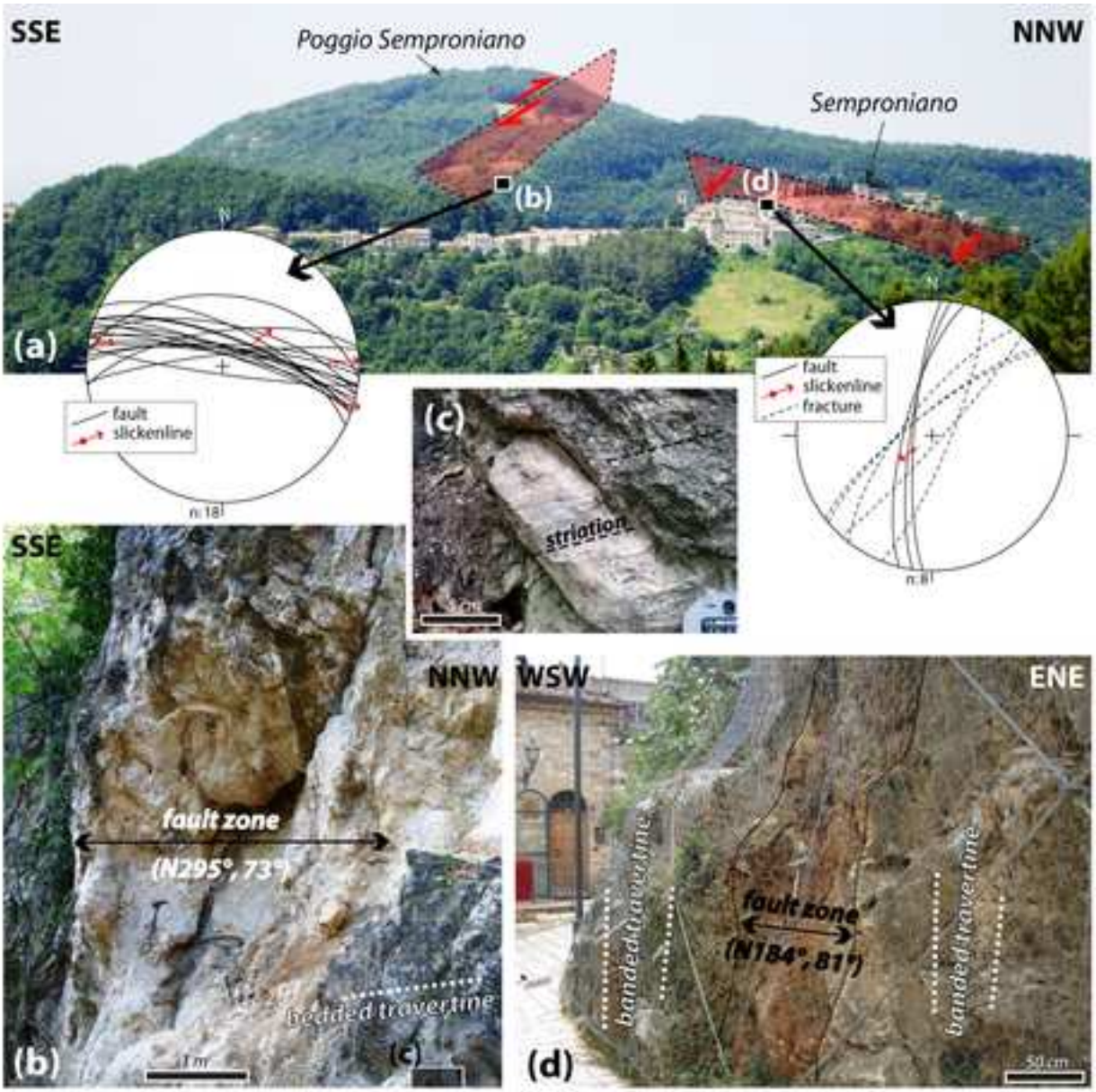

Figure 6. (a) Panoramic view of the Semproniano-Poggio Semproniano area where the traces of the main fault systems (*ca.* E-W- and N-S-striking) are indicated. The stereoplots (Schmidt net, lower hemisphere) show attitude of the measured structural features. **(b)** The E-W-striking fault system affecting the bedded travertine at Poggio Semproniano is characterized by meter-thick damage zone and narrowly-spaced fault surfaces. **(c)** Fault surfaces are equipped with oblique- to strike-slip striations (pitch is generally higher than 160° or lesser than 20°; see the stereoplot). Right-lateral strike-slip kinematics has been documented for this fault system. **(d)** The N-S-striking fault across the banded travertine of the Semproniano village is defined by a half-meter-thick damage zone and secondary fracture network. Extensional kinematics (associated to a left-lateral movement) has been documented for this fault system.

Figure 7
Click here to download high resolution image

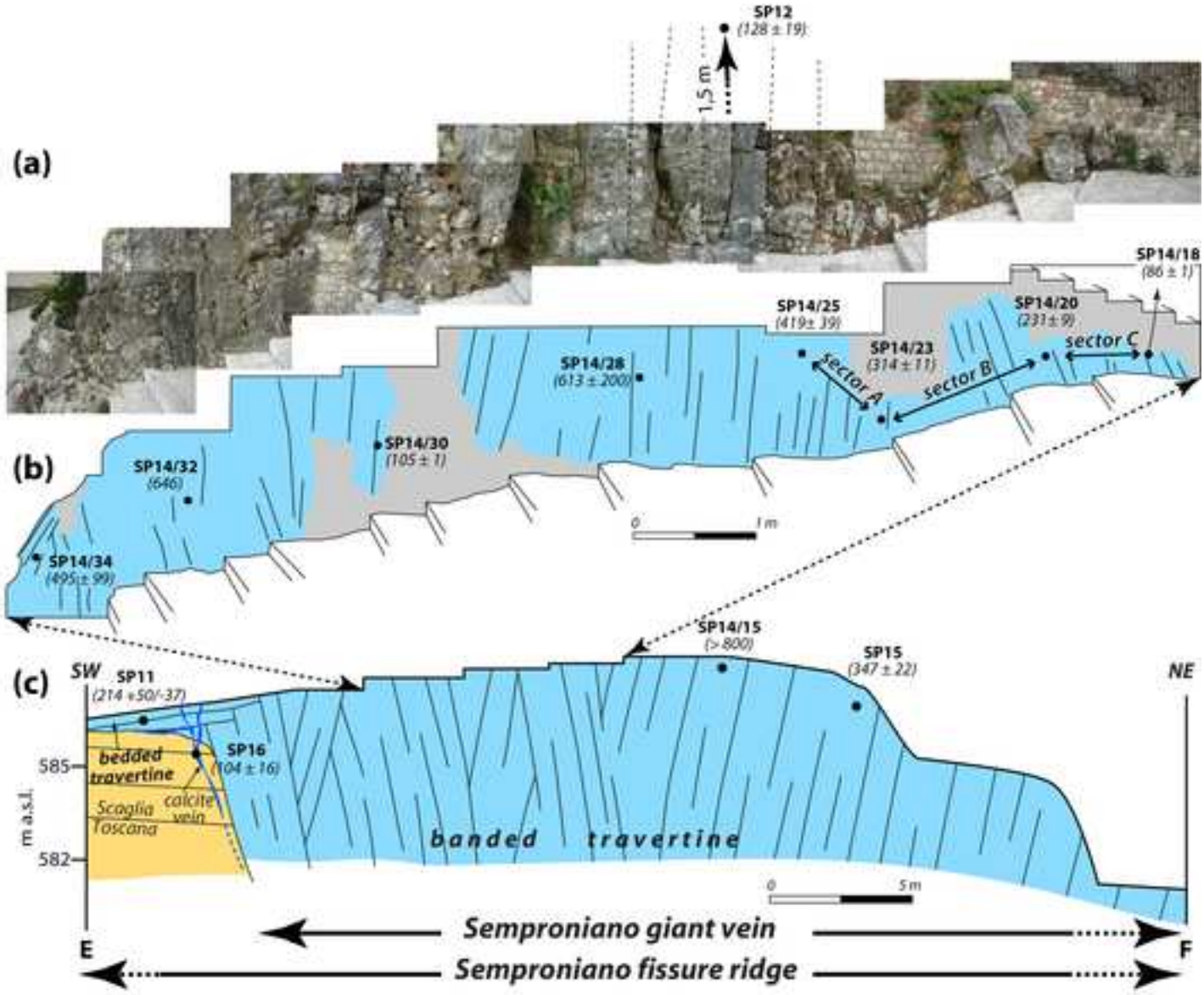

Figure 7. (a) Photomosaic (above) and related line drawing (below) of the Sempronian giant vein as it is exposed in the upper part of the Sempronian village. **(b)** Conceptual cross-sectional sketch of the Sempronian giant vein that is made of an uninterrupted swarm of sparry bands (banded travertine). Sample location and related radiometric ages are shown both in (a) and in (b).

Figure 8

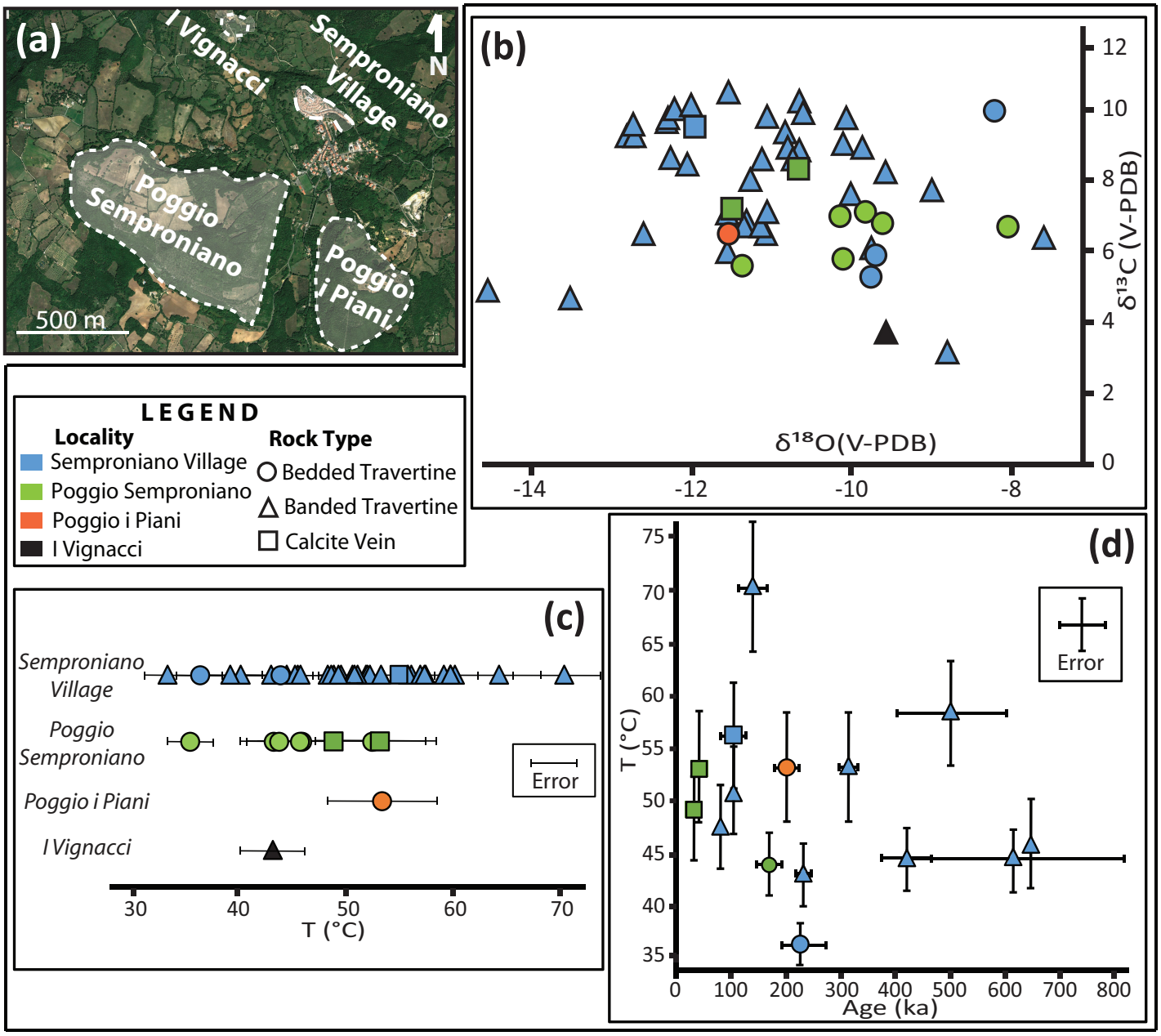

Figure 8. **(a)** Panoramic view (Google Earth image) with localization of the studied travertine deposits (same as Fig. 3a). **(b)** Combined plot of $\delta^{13}C$ (‰ V-PDB) and $\delta^{18}O$ (‰ V-PDB) isotope values derived from samples of bedded and banded travertines and calcite veins (Table 3). **(c)** Plot of calculated temperatures for the parental fluids of the studied travertines and $CaCO_3$ precipitates (Table 3). **(d)** Combined plot of parental fluid temperatures and U/Th ages determined on the same samples.

Figure 9

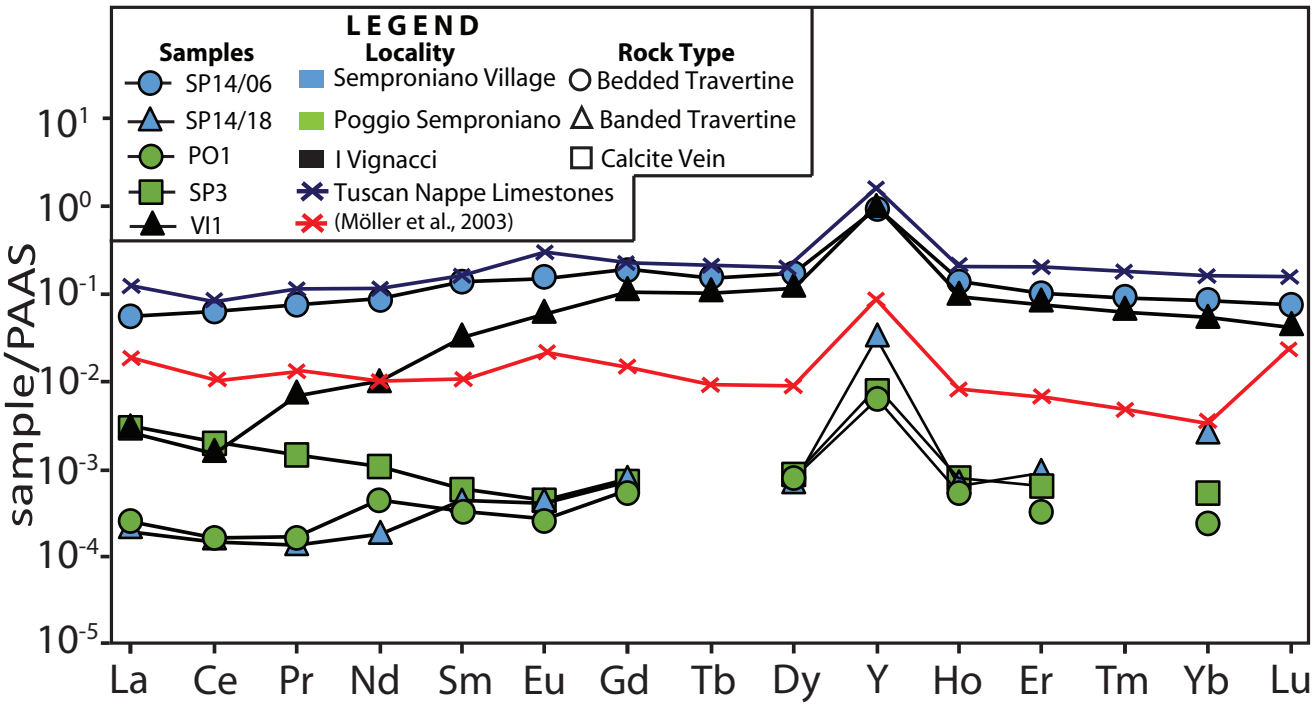

Figure 9. Post Archean Australian shale (PAAS) – normalized REY pattern (rare Earth elements + Yttrium) for: the Semproniano giant vein (banded travertine); the bedded travertine flanking the giant vein; bedded travertine and calcite vein from Poggio Semproniano; and banded travertine from I Vignacci. For comparison, REE data from the Tuscan Nappe limestone are also shown (data from Möller et al., 2003).

Figure 10

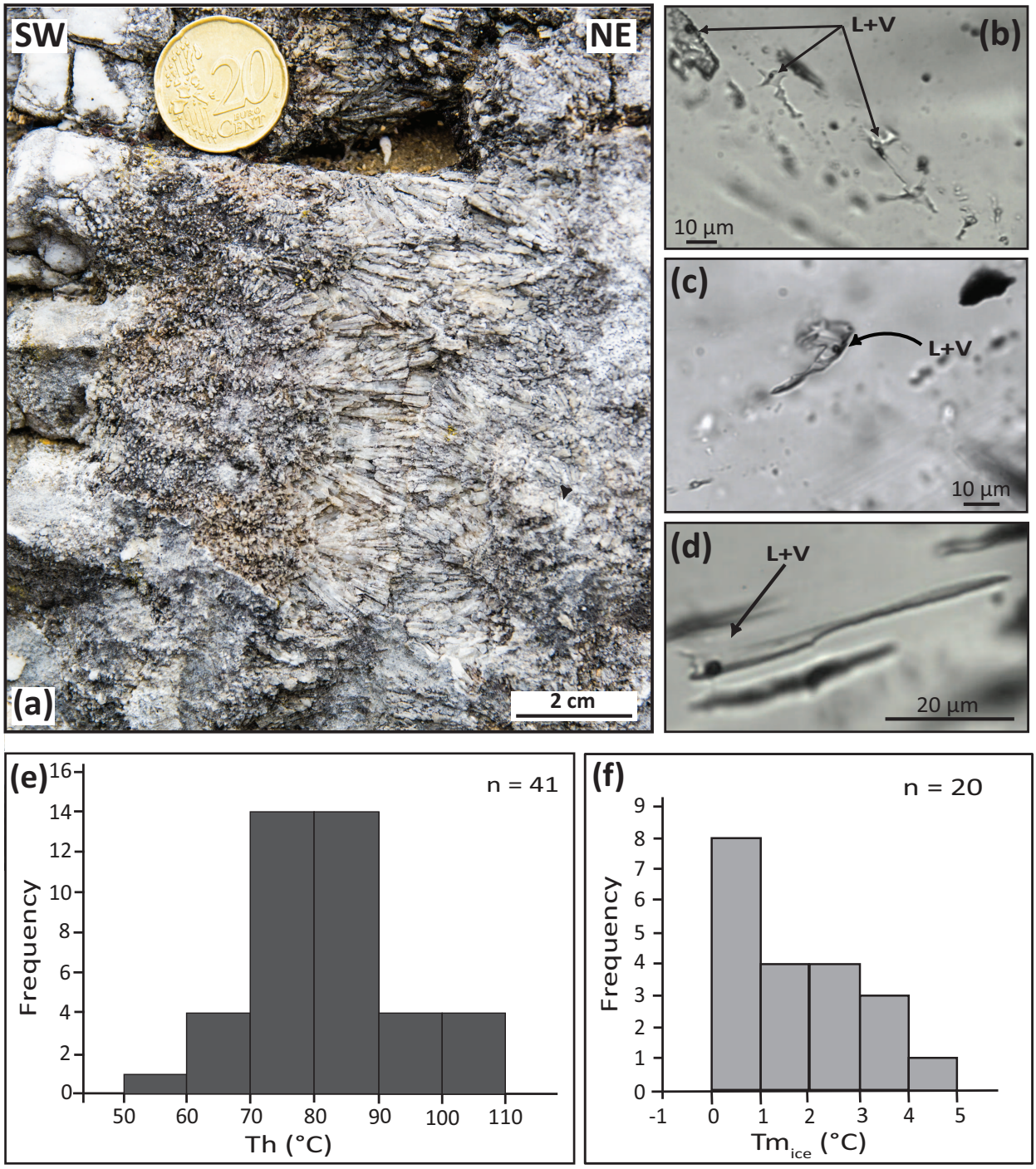

Figure 10. (a) Close up photograph of banded travertine from the central part of the Semproniano giant vein. The sample studied for fluid inclusions comes exactly from the spot shown in the photograph. **(b)**, **(c)**, and **(d)** Microphotographs (transmitted light, parallel nicols) of liquid-rich fluid inclusions hosted in the banded travertine shown in the previous close-up photograph. L and V are for liquid and vapor phases, respectively, within the studied inclusions. **(e)** and **(f)** Results of microthermometry on fluid inclusions hosted in elongate calcite crystals. Th is the temperature (°C) of homogenization whereas Tm_{ice} (°C) is the temperature of last melting of ice.

Figure 11
Click here to download high resolution image

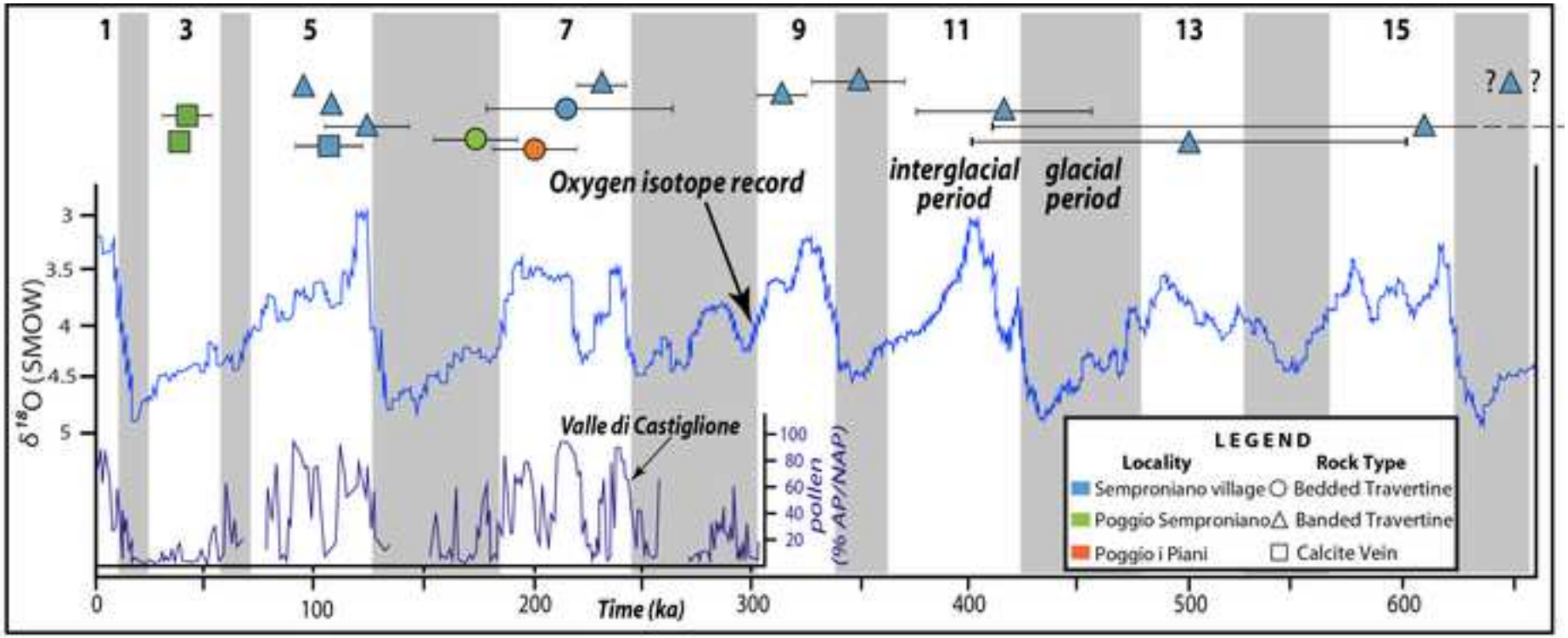

Figure 11. Comparison between U/Th ages of bedded travertine, banded travertine, and calcite veins from the study area and major paleoclimate indicators represented by the deep sea oxygen isotope trend (Zachos et al., 2001) and by the pollen dataset from Valle di Castiglione (Tzedakis et al., 2001). Global glacial/interglacial periods are redrawn and modified after Priewish et al (2014).

Figure 12
Click here to download high resolution image

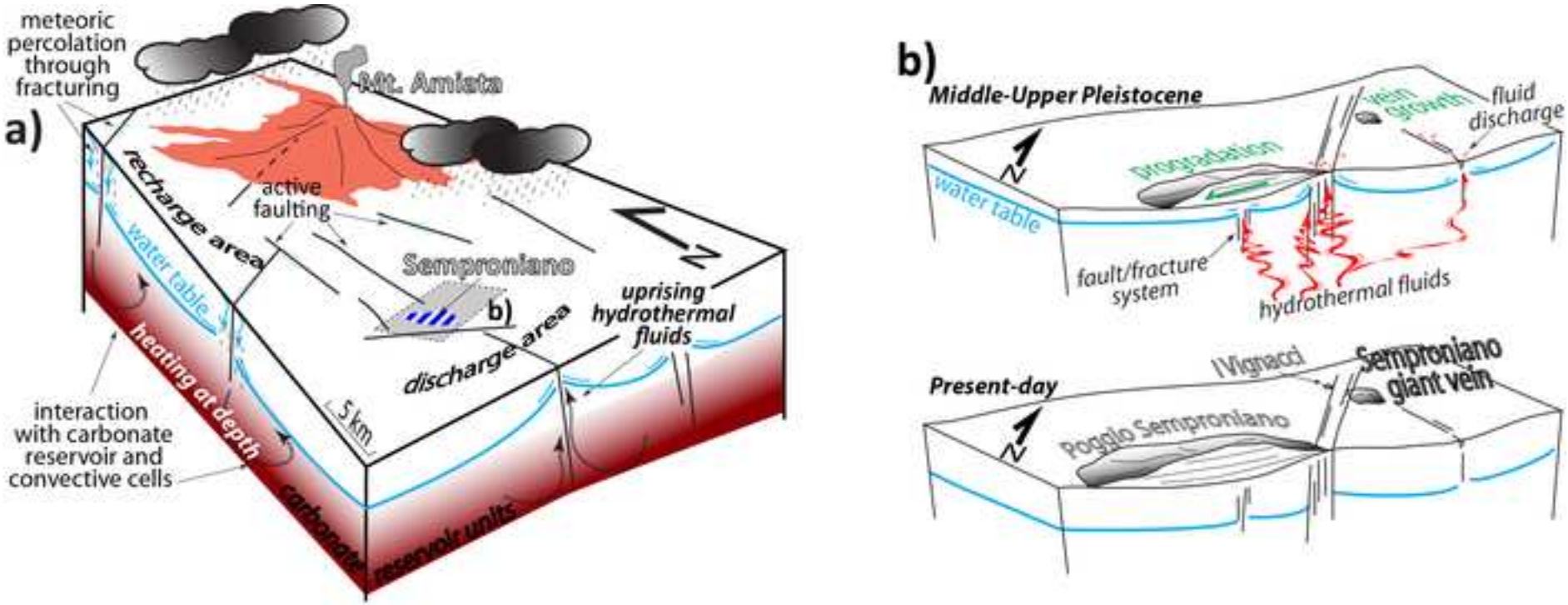

Figure 12. (a) Schematic 3D-block diagram interpreting the hydrothermal settingin the Mt. Amiata-Sempronianо area. Active faulting and related fracturation have primary role in controlling meteoric percolation within the carbonate reservoir at depth, and the uprise of hydrothermal fluids. **(b)** Two-step scenario illustrating the mode of travertine deposition (by veining at Sempronianо fissure ridge and by dominant progradation at the Poggio Sempronianо plateau) supplied by hydrothermal fluid discharge at the fault/fracture tips. The fault architecture is indicative.

Table S1

Click here to download Supplementary material for online publication only: Semproniano_TableS1_Berardi et al.docx

Table S2

Click here to download Supplementary material for online publication only: Semproniano_TableS2_Berardi et al.docx